UNIVERSITY OF SÃO PAULO

INSTITUTE OF CHEMISTRY

Graduate Program in Chemistry

THAYLAN PINHEIRO ARAÚJO

Catalysts based on Transition Metals for Applications in Energy Conversion

The original version of the dissertation

São Paulo

Deposit date at SPG

January 31st 2019

UNIVERSIDADE DE SÃO PAULO

INSTITUTO DE QUÍMICA

Programa de Pós-graduação em Química

THAYLAN PINHEIRO ARAÚJO

Catalisadores baseados em metais de transição para aplicações em processos de conversão de energia

Versão da dissertação corrigida

São Paulo

Data de depósito na SPG

31/01/2019

THAYLAN PINHEIRO ARAÚJO

Catalysts based on Transition Metals for Applications in Energy Conversion

Thesis Presented in the Chemistry Institute at the University of São Paulo in order to obtain the Master's degree in Science (Chemistry).

Advisor: Prof. Dr. Pedro Henrique Cury Camargo

The original version of the dissertation

São Paulo

2019

Autorizo a reprodução e divulgação total ou parcial deste trabalho, por qualquer meio convencional ou eletrônico, para fins de estudo e pesquisa, desde que citada a fonte.

Ficha Catalográfica elaborada eletronicamente pelo autor, utilizando o programa desenvolvido pela Seção Técnica de Informática do ICMC/USP e adaptado para a Divisão de Biblioteca e Documentação do Conjunto das Químicas da USP

Bibliotecária responsável pela orientação de catalogação da publicação:

Marlene Aparecida Vieira - CRB - 8/5562

A 658 c

Araújo, Thaylan Pinheiro
Catalysts based on Transition Metals for Applications in Energy Conversion. / Thaylan Pinheiro Araújo. - São Paulo, 2019.
82 p.

Dissertação (mestrado) - Instituto de Química da Universidade de São Paulo. Departamento de Química Fundamental.
Orientador: Camargo, Pedro Henrique Cury

1. Energy Conversion. 2. CO2 hydrogenation. 3. Water splitting. 4. Heterogeneous catalysts. 5. Earth-abundant Transition metal. I. T. II. Camargo, Pedro Henrique Cury, orientador.

UNIVERSIDADE DE SÃO PAULO
INSTITUTO DE QUÍMICA

"Catalisadores baseados em metais de transição para aplicações em processos de conversão de energia"

THAYLAN PINHEIRO ARAÚJO

Dissertação de Mestrado submetida ao Instituto de Química da Universidade de São Paulo como parte dos requisitos necessários à obtenção do grau de Mestre em Ciências - no Programa de Química.

Aprovado (a) por:

Profa. Dra. Susana Inês Córdoba de Torresi
(Presidente)

Prof. Dr. Mauro Coelho dos Santos
UFABC

Profa. Dra. Ana Flávia Nogueira
IQ - UNICAMP

SÃO PAULO
12 de fevereiro de 2019

To my parents, Rosa e Manoel, who have always unconditionally supported and loved me.

To my sister, Thaynara, who has always been there for me.

" Nothing in life is to be feared, it is only to be understood. Now is the time to understand more, so that we may fear less."

- Marie Sklodowska Curie

" The ones who aren't able to acknowledge their own selves are bound to fail."

- Itachi Uchiha

ACKNOWLEDGMENTS

First of all, I thank God for everything in my life and especially for giving me the strength that I need to always go beyond.

I would like to express my deepest gratitude towards my parents, Rosa and Manoel, and my sister, Thaynara. Without them I would never be able to complete this work or accomplish anything in my life. Thank you for always encouraging me to pursue my dreams. Also, thank you very much for your endless love and support. I love you all so much!

To my cousin, Andreia, and her husband, Audiel, for hosting me when I first got in São Paulo. I really appreciate everything you did for me. Thanks!

I would also like to thank my supervisor, Professor Pedro H. C. Camargo, for accepting me in his group. I am so grateful for the opportunity to work under his supervision. I really appreciate his trusting and believing in me. Thank you for all the opportunities, feedbacks, and advices you gave to me. Those have helped me a lot to shape my career and personal life. Finally, thank you very much for teaching me how to make the worst jokes ever. I will carry this knowledge with me forever.

I would like to thank Professor Susana I. C. de Torresi (IQ-USP) for kindly guiding me in the electrochemical part of this thesis. I really appreciate the time she spent patiently discussing my data with me and teaching me precious electrochemical concepts. Thank you very much for everything!

I would also like to thank Professor José A. Rodriguez (Brookhaven National Laboratory- US) for accepting me as a visiting student in his group. This was an exceptional opportunity in which I could develop and discuss my work with a brilliant scientist who inspired me to become more passionate about the field of catalysis. Thank you!

My special thanks to my GrAND colleagues and friends, who made me feel part of an outstandingly talented and fun scientific team: Duh, Paulo, Rafa, Maria, Luanna, Jhon, Helô, Ivonne, Ivo, Victor, Carmine, Maurício, Yukio, Rafael Geonmonond, Marcos, Igor, Gui, Livia, Isabela, Bárbara, Bel, Gabs, and Rodolfo.

I would like to thank my collaborators for helping me with their intellect, time and friendship. They have not only assisted me on developing this work, but broadened

my horizons to other equally exciting investigation fields: Luanna, Jhon, Duh, Jhonatan, Paulo, and Arthur. I would never get even half way I am without your help. Thank you!

From the bottom of my heart, I would like to thank the friends whom life has gave to me as precious gift during my journey. Duh, it is always so much fun talking to you and falling for your pranks. Paulo, you are such a big-hearted person who is always willing to listen to my boring talks and giving me the best advices. Rafa ("Bexta"), you are such an adventurous and kind person whose honesty and friendship are always welcomed. Maria (Mapa), you always come up with the best way to handle things, but we don't usually listen to you so that we end up doing the wrong thing, I will start listen to you more, I promise. Luh, you are such a good vibe and cheerful person who is always trying to cheer people up and help them. Jhon (Rapa), you are such a playful person who always help me whenever I need. Helô, you are such a calm and mature person who inspires me to become a little bit like you. Jhonatan, you are such a determined and bright person who is always willing to help everyone. Ivonne, you are such hard-working and kind person who always inspires me to be a little bit more like you. To all of you, my sincere gratitude. I would never be able to go smoothly through this journey without your friendship. THANK YOU VERY MUCH!

To my friends of IQUSP, Adriana and Diego, for being the piece of my beloved Nordeste in São Paulo. Thanks!

To my friends in Maranhão who always cheer me up to keep on pursuing my dreams: Mary, Jeovan, Yaucha, Bianca, Fabi, Bárbara, Wemerson, Welton, Gabriel, Elizaura, Mayara, Paulina, Josimar, Geyse and Profa. Ana. Thank you!

To my Irish/Brazilian family who always celebrate and encourage me to go on my next adventure: Marcela (Pimenta), Marlos (Idoso), Raíssa, Letícia, Milena, Érika, Glaucia (CRAUDIA), and Jhones. Thanks!

To all members of the Catalysis: Reactivity and Structure (CRS) Group at Brookhaven National Laboratory (BNL) for helping me during my internship: Luis, Lili, Zongyuan, Mausumi, Juan Pablo, Ivan, Nin, Siyu, Kaixi, Jindong, Rebecca, Feng and Fran (my good Brazilian friend who endured with me the isolation of living in BNL`s accommodation, we did it!). In particular, I would like to thank Dr. Sanjaya Senanayake for always asking me about my work, giving so many good advices to me, and teaching me a lot about how to become a good scientist.

To the Syncroton National Laboratory (LNLS) in Brazil, the Brookhaven National Laboratory(BNL), and the Advanced Photon Source (APS) in the USA for providing excellent experimental infrastructure, which was pivotal to the development of this work. Thank you!

To Profa. Liane Marcia Rossi, Prof. Roberto Manuel Torresi, and Prof. Erick Bastos Leite for opening their labs to us. Thank you!

To Neder and André from the Laboratório de Materiais Eletroativos - IQ-USP for always helping me with whatever and whenever I needed to work in their lab. Thank you!

To Dona Rosa for always taking care of our lab, making it a GrAND and enjoyable place to work in. Thank you!

To São Paulo Research Foundation (FAPESP) for the financial support, the Master fellowship (grant #2017/07564-8), and Research Internship Abroad (BEPE) fellowship (grant #2017/25882-7). Thank you very much!

To FAPESP, CAPES, CNPq and Serrapilheira Institute for the financial support to the GrAND nanolab. Thanks!

ABSTRACT

Araujo, T.P. **Catalysts based on Transition Metals for Applications in Energy Conversion.** 2019. 82p. Master's Thesis - Graduate Program in Chemistry. Institute of Chemistry, University Of São Paulo, São Paulo.

Energy conversion processes such as the water splitting and CO_2 hydrogenation reactions have emerged as attractive approaches to mitigate environmental concerns on CO_2 emissions as well as to provide an alternative source of renewable fuels. These strategic processes can capitalize on the energy of renewable resources (e.g solar and wind) to drive chemical reactions to generate, in a green and sustainable way, fuels and value-added chemicals. Economically feaseable heterogeneous catalysts play a central role in advancing such processes for globally-relevant production scales. Hence, in this work, we focused on the synthetic development of several catalyst systems based on cost-effective earth-abudant 3d transition metals such as nickel (Ni), cobalt (Co), iron (Fe) and zinc (Zn). Specifically, we turned our attention to produce a series of catalysts comprised of: *i*) NiFe oxyhydroxide supported on carbon for application in oxygen evolution reaction (OER), a bottleneck reaction for the water splitting process, and *ii*) Ni and Co nanoparticles supported on Zinc oxide (ZnO) for the CO_2 hydrogenation reaction. Regarding the NiFe oxyhydroxide systems, we evaluated the catalytic performance of these materials towards the OER and benchmarked those with that of state-of-the-art OER electrocatalyts such as Ir/C. In addition to that, we also focused on rationalizing the key reasons for the significant enhancements in OER activity of such catalysts in terms of their surface and bulk compositions. For Co/ZnO and Ni/ZnO catalysts, aside from assessing their catalytic activity and selectivity behavior, we performed a systematic investigation of the catalytically important properties of such catalyst interfaces under typical CO_2 hydrogenation reaction conditions using *in situ* ambient pressure X-ray photoelectron spectroscopy (AP-XPS). This allowed us to acquire important knowledge into the origin and the nature of the active sites associated with the catalytic activity and selectivity in these materials.

Keywords: Energy Conversion; CO_2 hydrogenation; Water splitting; Heterogeneous catalysts; Earth-abundant Transition metals.

RESUMO

Araújo, T.P. **Catalisadores baseados em metais de transição para aplicações em processos de conversão de energia.** 2019. 82p. Dissertação de Mestrado – Programa de Pós-Graduação em Química, Instituto de Química, Universidade de São Paulo, São Paulo.

Processos de conversão de energia, como as reações de quebra de água e hidrogenação de CO_2, têm surgirdo como abordagens atraentes para mitigar as preocupações ambientais das emissões de CO_2, bem como para fornecer uma fonte alternativa de combustíveis renováveis. Esses processos estratégicos podem capitalizar a energia de recursos renováveis (por exemplo, solar e eólica) para realizar reações químicas que geram, de forma sustentável e ecológica, combustíveis e produtos químicos com valor agregado. Catalisadores heterogêneos economicamente viáveis desempenham um papel central no avanço de tais processos para escalas de produção globalmente relevantes. Assim, neste trabalho, nos concentramos no desenvolvimento sintético de vários sistemas catalisadores baseados em metais de transição 3d abudantes como o níquel (Ni), cobalto (Co), ferro (Fe) e zinco (Zn). Especificamente, voltamos nossa atenção para produzir uma série de catalisadores compostos de: i) oxi-hidróxido de NiFe suportado em carbono para aplicação na reação de evolução de oxigênio (OER), uma reação limitante para o processo de quebra de água, e ii) nanopartículas de Ni e Co suportadas em Óxido de zinco (ZnO) para a reação de hidrogenação do CO_2. Com relação aos sistemas de oxi-hidróxido de NiFe, avaliamos o desempenho catalítico desses materiais frente a OER e comparamos estes com eletrocatalisadores para OER de última geração, como Ir/C. Além disso, também nos concentramos em racionalizar as principais razões para as melhorias significativas na atividade catalítica de tais catalisadores em termos de suas composições de superfície e volume. Para os catalisadores de Co/ZnO e Ni/ZnO, além de avaliar sua atividade catalítica e seletividade, realizamos uma investigação sistemática *in situ* das propriedades cataliticamente importantes de tais interfaces usando a Espectroscopia de Fotoelétrons de Raios X a Pressão Ambiente. (AP-XPS) sob condições típicas de reação de hidrogenação de CO_2. Isso nos permitiu adquirir conhecimentos importantes sobre a origem e a natureza dos sítios ativos associados à atividade e seletividade catalítica nesses materiais.

Palavras-chave: Conversão de energia; Hidrogenação de CO_2; Separação de água; Catalisadores heterogéneos; Metais de transição abundantes na Terra.

TABLE OF CONTENTS

1. INTRODUCTION

1.1 Energy Conversion

At present, we are undeniably facing a carbon dilemma. Globally increasing energy demands have continuously intensified the consumption of our main energy source, the fossil fuels reserves.[1,2] And the burning of such diminishing reserves has been accompanied by inexorable anthropogenic carbon dioxide (CO_2) emissions that are outpacing nature's CO_2 recycling capability, thus triggering substantial environmental concerns.[2–5] Due to this scenario, ever-growing research efforts have been dedicated to develop new energy systems that are sustainable, clean, low cost, and environmentally benign. [1,2,4–6]

Several strategies have been proposed to reshape such disturbing scenario. In this context, exploiting renewable resources have shown to be the most promising one. Examples those energy technologies based on wind, solar, and hydroelectric, which have been expanding throughout the past 50 years.[1,2,7] While these technologies hold great promise to replace fossil fuels as cleaner, environmentally safer and sustainable energy sources, the fact that they are diffuse and intermittent energy supplies poses a fundamental challenge that must be overcome before placing them as the basis of our global energy system.[1,2,8]

Of importance to overcome such drawback is an approach that capitalizes on the energy of such intermittent resources by storing it in an efficient and cost-effective manner in chemical bonds. That is, the energy can be used to drive chemical reactions to generate, for example, hydrogen (H_2) fuel and, by recycling CO_2, other fuels or value-added chemicals.[6,9,10] Both of these molecular systems have become the most

reasonable and appealing prospects for the efficient storage of renewable energy.[4,7,11,12] In particular, because these storable forms of energy can be utilized on demand, which is a highly desired in order to complement the intermittent energy gaps of renewable sources. [6,9] Furthermore, this type of approach offers an outstanding close loop to the gigantic and increasing amount of CO_2 emissions, which can, on a short to medium term, contribute to meeting global strict emission regulations as well as to providing a new worldwide network of renewable fuels. As a result, this would provide a proper way to overcome a future energy supply shortages and to mitigate environmental concerns.[4,11–13]

1.1.1 Water Splitting Process

Hydrogen is considered to be an excellent fuel given its similar performance and operation to fossil-fueled technologies.[14–16] As such, it plays an important role in the provision of electricity and heat for industry and transportation worldwide.[14–17] To an industrially point of view, H_2 production is already a well-established large-scale process in which two of the currently main pathways for its production are steam methane reforming ($CH_4 + 2H_2O \rightarrow 4H_2 + CO_2$) and coal gasification ($C + 2H_2O \rightarrow 2H_2 + CO_2$).[15,16] Even though these pathways together are responsible for supplying more than 95% of the global hydrogen production, they use mainly fossil-fuels as feedstock and generate the greenhouse CO_2 as byproduct.[14,15] Thus, these processes do not offer a good choice towards the transition to a greener and sustainable low-carbon economy.

Compared to those, only 4% of the hydrogen is produced by water electrolysis.[15] However, such water splitting process ($2H_2O \rightarrow 2H_2 + O_2$) provides hope that it is

possible to shift in global hydrogen production from the current fossil fuel-based methods to a sustainable approach by utilizing water as an abundant feedstock and a renewable hydrogen source.[14,15,18,19] Despite its attractive features, water splitting is a thermodynamically nonspontaneous process with a positive Gibbs free energy change of 286 kJ mol^{-1} at room temperature and pressure.[20,21] Thus, a significant energy input is required for such uphill process to produce H_2, which can severely increase production costs and, in turn, limit its eventual industrial implementation.[14,15]

Electrochemical water splitting is beheld as an efficient and scalable alternative to address such significant challenge.[20–23] This is because it can straightforwardly exploit electric power generated from low-cost and renewable energy sources such as the sun, wind, or others to drive H_2 production.[12,21,23,24] In such water splitting system, a photovoltaic (PV) cell, for example, is connected to a separate electrolyzer with catalysts that can drive the desired conversion reactions (**Figure 1a**).[20,25] This system is typically identified as PV/electrolysis.[20,25] Another promising setup is based on a fully integrated system known as photoelectrochemical (PEC) cell (**Figure 1b**). In such device, solar absorbers (e.g semiconductors) are coated with efficient catalysts to generate photoelectrodes that can perform the desired chemical transformations.[20,25,26] In many aspects, PV/electrolysis devices are much more advanced and mature technologically than the corresponding PEC devices. For instance, the latter requires effective integration of the photon absorber and the catalyst in order form them to achieve desired conversion efficiencies.[20,25,26] Another reason is that PV/electrolysis devices rely on conventional and tried-and-tested technologies (e.g. solar cells). This has helped

them attaining more efficient performances relative to PEC devices thus far.[20,25]

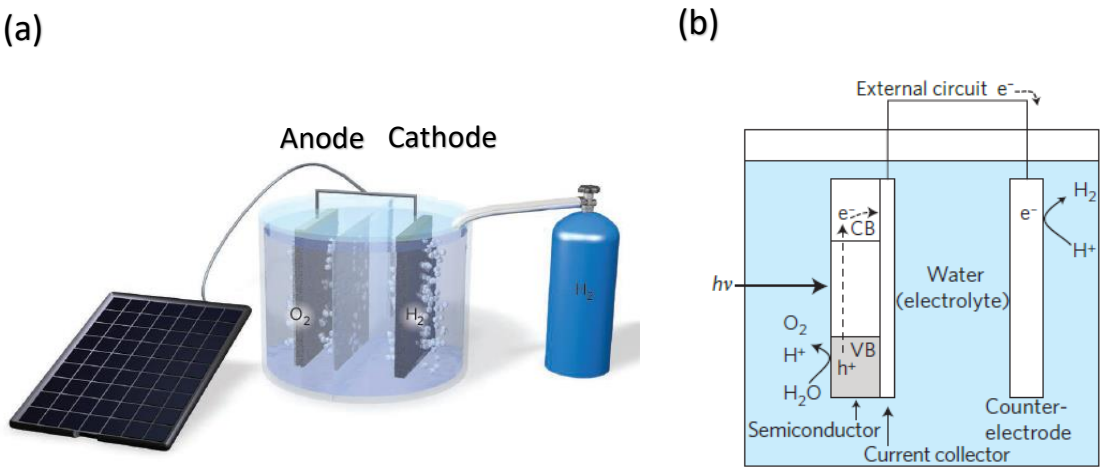

Figure 1. Representative diagrams of electrochemical water splitting devices. (a) PV/electrolysis device; (b) Photoelectrochemical cell design. In both devices, water splitting redox half-reactions, the oxygen evolution ($2H_2O \rightarrow O_2 + 4H^+$) and hydrogen-evolution ($2H^+ + 2e^- \rightarrow H_2$), take place at the anode and cathode, respectively.[25,27]

In addition to some technical and operational shortcomings of either PV/electrolysis and PEC devices, two key elements that greatly affect the efficiency of the overall water splitting process in both devices are the hydrogen (HER) and oxygen (OER) evolution reactions.[21,28] For electrolytic cells, HER and OER occur at the cathode and the anode, producing gaseous H_2 and O_2 molecules, respectively (**figure 1a**). When combined, these two half reactions result in a thermodynamic potential of $E^0 = -1.23$ V.[21,28] Nonetheless, their nature can differ depending on the solution pH as illustrated in **figure 2**. However, either at very high or very low pH, at which the concentration of charge carriers is greatest, is desired for achieving high performance in conventional electrolysis.[9,20,21]

In aqueous acid:

$$OER:\ \ 2H_2O\ (l)\ \rightarrow\ O_2(g)+\ 4H^+ +\ 4e^- \qquad E^0 = -1.23V$$

$$HER:\ 4H^+ +\ 4e^-\ \rightarrow\ 2H_2(g) \qquad E^0 = 0.00V$$

$$Overall: 2H_2O\ (l)\ \rightarrow\ O_2(g)+\ 2H_2(g) \qquad E^0 = -1.23V$$

In aqueous base:

$$OER:\ 4OH^-\ \rightarrow\ O_2(g)+\ 2H_2O\ (l)+\ 4e^- \qquad E^0 = -0.40V$$

$$HER:\ 4H_2O\ (l)+\ 4e^-\ \rightarrow\ 2H_2(g)+\ 4OH^- \qquad E^0 = -0.83V$$

$$Overall: 2H_2O\ (l)\ \rightarrow\ O_2(g)+\ 2H_2(g) \qquad E^0 = -1.23V$$

Figure 2. Representation of Water-Splitting Half Reactions at Low and High pH. Adapted from reference 21.

In general, the kinetics of the two-electron transfer process for the formation of H_2 in the half-cell HER process is reasonably simple. In contrast, OER is a kinetically sluggish reaction due to its multi-electron transfer nature and significant molecular rearrangement required during the reaction.[9,21] This results in a much slower kinetics compared to that of the HER. Hence, overall efficiency of water-splitting systems is greatly limited by the performance of the OER process.[9,22–24] In this sense, as the OER not only plays a crucial role in such systems but also in energy storage devices (e.g. metal–air batteries), ever-increasing efforts have been devoted towards developing stable and highly active catalysts for such reaction that, in turn, can improve water splitting efficiency as a whole process. [9,22–24,29]

1.1.2 Hydrogenation of Carbon Dioxide (CO_2)

Curbing CO_2 emissions by recycling this greenhouse gas into fuels or value-added chemicals (e.g. CH_3OH, CH_4, HCOOH, CO, and CH_3CH_2OH) offers an outstanding approach

to circumvent the gigantic and increasing amount of CO_2 emissions. This, in turn, can contribute to alleviating the effects of climate change, and yet to provide a remarkable way to make renewable fuels.[4,13,30] Although this represents an excellent and sustainable approach, the path towards making fuels from CO_2 on a technically feasible, large-scale, and economically competitive way is highly complex. This occurs as a result of some particularities of the recycling process.[12,31,32] For example, CO_2 is well-known to be a highly stable molecule (ΔG_f° = −396 kJ/mol), which is the end product of several combustion processes. [12,32] Hence, converting it into fuels or other chemicals requires a significant amount of energy that depends on the oxidation state value of carbon in the target chemical or fuel. Moreover, the conversion process requires technologies that need to be efficiently scaled up to handle hundreds of megaton of carbon dioxide. [13,31,33]

Remarkably, CO_2 hydrogenation process has emerged as a pioneering approach for targeting and accelerating such CO_2 utilization strategy.[4,13,31] This process can be straightforwardly adapted into existing chemical and petrochemical industrial infrastructure. [12,13] Thus, it holds promise to produce volumes of desired chemicals and fuels at globally significant scales. Another reason is that this process is a self-sustainable and environmentally friendly. For instance, it relies on molecular hydrogen (H_2) as a reducing agent, which can be provided by various renewable sources. [12,31] Moreover, sunlight energy can be indirectly harnessed by solar concentrators to generate heat, which can then be used to convert CO_2 into fuels using thermochemistry.[34]

This promising route to producing fuels and chemicals from gaseous CO_2 can be attained through a variety of known reactions (**figure 3**). Methanol synthesis represents one of the most desirable option for CO_2 utilization, as it generates a liquid feedstock that is excepicionally convenient for producing olefins and fuels.[35,36] However, its

impact alone on global reduction of CO_2 emissions is not quite significant (its CO_2 consumption is limited to lower than 0.1%).[36,37] Aside from methanol, reverse water gas shift (RWGS) and CO_2 methanation reactions can generate other chemicals such as carbon monoxide (CO) and methane (CH_4), respectively, which are important building blocks for a wide range of commodities.[36,38,39] For instance, a variety of products such as olefins, gasoline, and diesel, as well as oxygenates (e.g. methanol) can be obtained from syngas (CO + H_2) using the well-established technology of Fischer–Tropsch synthesis (FTS).[40–42] In this way, both RWGS and CO_2 methanation reactions offer an exciting way to expanding the scope of products to be manufacted from the hydrogenation of CO_2, complementing that of direct methanol synthesis, and therefore contributing to a more effective utilization of CO_2.[34,43]

$$\boldsymbol{Reverse\ Water\ Gas\ Shift}: \quad CO_2\,(g) + H_2(g) \rightarrow H_2O(l) + CO(g)$$

$$\boldsymbol{CO_2\ Methanation}: \quad CO_2\,(g) + 4H_2(g) \rightarrow 2H_2O(l) + CH_4(g)$$

$$\boldsymbol{Methanol\ Synthesis}: \quad CO_2\,(g) + 3H_2(g) \rightarrow 2H_2O(l) + CH_3OH(l)$$

Figure 3. Three main pathways for industrial CO_2 hydrogenation process. Adapted from reference 34.

Even though this hydrogenation methodology holds several advantages, it has not yet reached its full potential. This is due to the fact that current heterogeneous catalysts still lack the required high activity, selectivity, and stability that can drive tomorrow's CO_2 hydrogenation refineries with an environmentally friendly energy balance, economic flow, and carbon footprint. [7,31,44] There is, therefore, an urgent need to improve or even discover materials with superior catalytic performances.

1.2 Catalysts for Energy Conversion

Regardless of the remarkable prospective of water splitting and CO_2 hydrogenation technologies for energy conversion purposes, several challenges must still be overcome for them to become a viable option and thus finally live up to their potential. One of the most important of these challenges is to develop highly selective and active catalysts to significantly improve the efficiency of such processes.[9,15,25,28,45]

Historically, catalysts have been playing a pivotal role in establishing a wide range of strategic energy- and atom-efficient sustainable chemical technologies.[10,43,46] It thus comes as no surprise that they play a key role in such uphill chemical transformations like water splitting and CO_2 hydrogenation.[20,34,45] This can be achieved by improving the kinetics of these reactions, offering less demanding energetic reaction pathways. [6,9,20,21,28,43]

Conventionally, heterogeneous catalysts based on noble metals are more commonly used to catalyze these chemical transformations.[6,9,43,47] These catalysts benefit such processes especially with their recognized long-term recyclability as well as by delivering satisfactory reaction rates.[12,31,33,48] However, their cost greatly hinder cost-effectiveness operations at global scales. [8,20,21,49] Therefore, endeavors toward heterogeneous catalyst development have concentrated over the last decades to designing catalysts using earth-abundant elements.[8,20,21,49] We believe that they represent a key step towards the development of new and economically feasible catalytic systems for clean and sustainable energy production. [6,20,46]

1.2.1 Nickel-Iron (NiFe) hydroxides for the Oxygen Evolution Reaction (OER)

The overpotential of a redox reaction is the potential above the thermodynamic potential needed to overcome reaction activation barriers.[21] In the case of the oxygen evolution reaction (OER), which provides protons and electrons to be used to generate H_2 fuel, it generally displays a quite large overpotential compared to HER.[17,20,21] Thus, particular focus has been placed on designing highly active electrocatalysts to lower the energy barrier of this essential reaction to the H_2 production. [9,20,21]

Commercial water splitting electrolyzers operate in highly conductive medium, that is, either in acidic or alkaline conditions.[17,50] In such conditions, both ruthenium oxide (RuO_2) and iridium oxide (IrO_2) are regarded as benchmark electrocatalysts for OER due to their high electrocatalytic activities.[17,50] However, despite exhibiting substantial stability in acidic medium, these catalysts suffer from a similar issue. They have a tendency to be oxidized and dissolved under high anodic potential during OER in both electrolytes.[17,50] In addition, both of them are based on noble metals, which are not suitable for realizing water spitting at large-scale production.[17,20,21,50] In this scenario, to reach the next level of technological advancement for the OER, special emphasis has been placed on non-precious metal-based OER electrocatalysts. [9,20,21,50]

The majority of these alternative materials are mostly investigated for application in standard alkaline electrolysers.[17,50,51] This is specially motivated by the cost-effectiveness and long-term stability of such catalysts on these devices.[17,50,51] Also, non-precious metal-based OER electrocatalysts tend to gradually or rapidly degrade in acidic medium.[17,21,51] Among the various earth-abundant OER catalysts developed so far (including perovskites[52–54], transition-metal oxides[55,56], and sulfides[57,58]), NiFe

oxyhydroxide (NiFe-LDH) materials are among the most promising active OER catalysts in alkaline electrolyte at low overpotentials.[22–24,29]

NiFe-LDH can be considered as a multicomponent system in which Fe^{3+} cations are doped in the neutral layers of Nickel hydroxides ($Ni(OH)_2$).[29,51] This results in a typical structure with Fe^{3+} centers surrounded and atomically isolated by Ni^{2+}sites, forming the oxygen bridged metal motifs of only Ni-O-Fe.[51,59] Moreover, this also gives rise to positively charged layers being originated and charge-compensated by anion intercalation in the interlayer region as illustrated in **figure 4a**. [29,51] Regarding the crystal structure, NiFe-LDH materials are isostructural with hydrotalcite and can be expressed with the chemical formula described in **figure 4b**.[24,51]

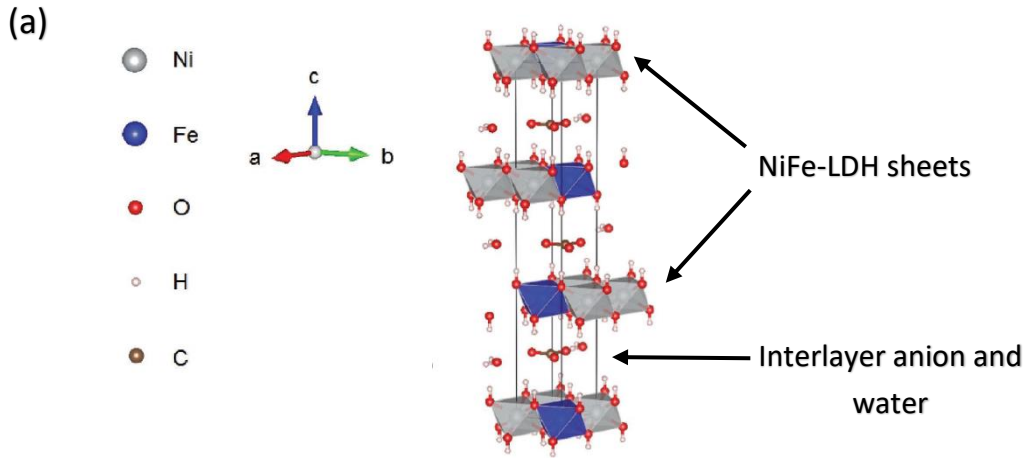

Figure 4. (b) Hydrotalcite-like NiFe LDH with intercalated water and carbonate anions (randomly distributed). (b) NiFe-LDH chemical formula, where x is the molar ratio of Fe that is incorporated, A is the anion, n is the charge of the anion and y the amount of water that is intercalated. Adapted from reference 51.

The promoting effect of Fe on $Ni(OH)_2$ OER catalytic activity was first discovered by Corrigan[60] in the 1980s and recently further highlighted by Trotochaud *et al.*[61] and Klaus *et al*.[62]. Although it is still highly debatable the precise roles played by Fe and Ni in the NiFe-LDH systems during OER, the incorporation of Fe in such systems have shown to be fundamental to lower the overpotential of $Ni_{1-x}Fe_x(OH)_2$ during OER, and therefore to increasing OER activities.[29,51,61,62] In fact, this has lead such electrocatalysts to achieve overpotentials in some cases lower than 200mV.[59] In this scenario, it is not surprising that much research efforts have been directed toward optimizing the intrinsic activity of NiFe-LDH.[17,29,51,63] In this case, reducing the particle size or delamination of Ni-Fe oxyhydroxide nanosheets have been the most common approaches.[29,64] Particularly, as they can increase the electrochemically available active surface area (ECSA), which is highly desired for improving electrocatalytic activity towards OER. [29,51,64,65] However, even with the good results from these strategies, several challenges remain on the way towards harnessing the high activity of Ni-Fe oxyhydroxide systems. Of particular interest is to obtain materials with enhanced charge transport and more abundantly exposed active sites.[23,24,64,65] To address such demands, some reported methodologies have focused on coupling pre-synthesized Ni-Fe oxyhydroxides and carbon nanomaterials (e.g graphene and carbon nanotubes) into hybrid catalyst materials. This strategy has shown to increase the number of exposed catalytic sites and accelerate charge-transfer kinetics, resulting in greatly enhanced OER performances.[23,24,64,65] It should be noted that the attractive generality and potential of this approach offer numerous opportunities to further driving the technological innovations that are needed to attaining high active OER Ni-Fe oxyhydroxide-based catalysts.

1.2.2 Non-Noble Metals Supp orted Zinc Oxide (ZnO) for CO_2 Hydrogenation

Owing to their electronic, chemical and catalytic properties, metal oxides can act as catalytic active phase, promoter, or "support" in chemical transformations.[66–69] These fundamental characteristics can be regarded as a main reason for the vast number of industrially relevant catalysts to be comprised of metal oxides. In fact, heterogeneous catalysts based on metal oxides play a central role in industrial production of numerous types of chemicals and materials that are worth billions of dollars. [68,70,71]

Zinc oxide (ZnO) has received tremendous interest lately.[72–74] This material is widely used in many applications, including catalysis and solar cells.[74–76] Its most thermodynamically stable phase is the wurtzite structure in which one Zn^{2+} ion is surrounded by four O^{2-} ions and vice versa giving rise to a tetrahedrally coordinated structure.[74,77] The particular interest for ZnO stems from the fact that it is an inexpensive and abundant material which has been employed in a number of important industrial applications,[72,74,78] such as the water-gas shift reaction[79,80], methanol synthesis[72], and the direct synthesis of light olefins from syngas.[81,82]

In the context of CO_2 hydrogenation, rather than ZnO alone, metal/ZnO interfaces have found to be of critical importance to achieve high performances. When it comes to methanol synthesis ($CO_2 + 3H_2 \rightarrow CH_3OH + H_2O$), $Cu/ZnO/Al_2O_3$ is the most commonly used catalyst. This benchmark catalyst display an excellent performance for methanol synthesis under elevated pressures of CO_2 and H_2..[72,83,84] It has been generally accepted that synergistic effects between ZnO and copper (Cu) nanoparticles play a crucial role to form the catalytic active phase in these systems.[72,83,85]

In light of importance of this catalyst system for CO_2 hydrogenation, special interest has been placed on optimizing its configuration for the conversion of CO_2 into other valuable chemicals aside from methanol. However, despite the fact that $Cu/ZnO/Al_2O_3$ catalyst is selective towards CO at ambient pressure conditions, Cu can lead to low CO_2 conversion.[86,87] Low-pressure CO_2 hydrogenation processes are more economically attractive with lower installation and operation (pumping) costs. Thus, a key approach to achieve an effective utilization of CO_2 via both RWGS and CO_2 methanation at such working conditions is replacing Cu with more active, but non-precious, metal components.

Several studies using other oxide-supports have shown that earth-abudant 3d transition metals such as cobalt (Co) and nickel (Ni) are promising canditates for achieving such goal.[36,38,88–91] However, the promotional effects of ZnO, which is known to possess extensive vacancy defects that can affect its interactions with supported nanoparticles, in CO and CH_4 synthesis over Co/ZnO or Ni/ZnO catalysts have not yet been addressed and thus are still not fully understood. [66,92] Therefore, it is pivotal not only evaluate the catalytic performance but rather to obtain fundamental understanding of structure–activity relationships of such catalyst materials under reaction conditions. In this way, one can acquire knowledge about basic questions concerning the nature of the active sites and the reaction mechanisms. With this, it is possible to further advance in the design and optimization of the next generation of highly active and selective earth-abundant metal-based heterogeneous catalysts for CO_2 hydrogenation. [48,93–95]

2. OBJECTIVES

Inspired by the challenges discussed in the previous sections, the main objective of this work is to develop and investigate catalysts comprised of earth-abundant 3d transition metals such as nickel (Ni), cobalt (Co), iron (Fe), and zinc (Zn) that can display enhanced catalytic performances for application in energy conversion processes. More specifically, we chose to focus on the oxygen evolution reaction (OER) and the hydrogenation of CO_2 as target transformations.

In order to address these challenges, several specifics goals were established.

- **Oxygen evolution reaction (OER):**

I. To develop a facile solvothermal synthesis method to obtain carbon hybrid Ni-Fe oxyhydroxides catalysts with different Ni/Fe ratios;

II. To study the catalytic performance of these materials towards the OER, comparing those with that of state-of-the-art OER electrocatalyts such as Ir/C;

III. To rationalize the catalytic performance of these materials in terms of surface and bulk composition;

- **CO_2 hydrogenation process:**

IV. To synthesize two series of ZnO-supported powder catalysts containing various amounts of Co or Ni NPs loadings;

V. To evaluate the catalytic activity and selectivity behavior of both series of catalysts under the RWGS or CO_2 methanation reactions;

VI. To carry out an *in situ/operando* Ambient Pressure X-Ray Photoelectron Spectroscopy (AP-XPS) systematical investigation of such catalytic surfaces. With this, we specifically aim at i) identifying and characterize the catalytically active sites of our catalysts under reaction conditions; ii) probing the influence of the

chemical and electronic nature of our support material on the catalyst reactivity and selectivity; and iii) building a correlation between surface chemistry of active catalysts and their corresponding catalytic performances.

3. MATERIALS AND METHODS

3.1 NiFe-electrocatalysts for Oxygen Evolution Reaction

3.1.1 Materials

Nickel(II) chloride hexahydrate ($NiCl_2$. $6H_2O$, 98%), Iron (II) sulfate heptahydrate ($FeSO_4$. $7H_2O$, 99%), Dimethylformamide (DMF, 99.9%), Ethanol (EtOH, 99%), Urea (99%) and Acetone (99%) were purchased from Synth, Brazil. Citric acid ($C_6H_8O_7$, 99.5%), Sodium hydroxide (NaOH, 98%), Potassium Hydroxide (KOH, 90%) and Nafion perfluorinated resin solution (5wt% in lower aliphatic alcohols and water) were obtained from Sigma-Aldrich. Carbon black (Vulcan XC72R) and 20wt% Ir/C (Iridium nanoparticle supported on Vulcan XC72R) were purchased from Cabot. All materials were used as received without any further purification.

3.1.2 Preparation of Ni-Fe catalysts

Ni, Fe and Ni-Fe catalysts were synthesized using a solvothermal methodology. In a typical procedure, 0.026mols of citric acid, 0.167mols of urea, (0.026-x)mols of $NiCl_2.6H_2O$ and xmols of $FeSO_4$. $7H_2O$ (x = 0.000, 0.0026, 0.0065, 0.013 and 0.026mols) were added to 50mL of DMF and sonicated for 30 min. Afterwards, the reaction mixture was transferred to a 130mL teflon-lined stainless steel autoclave, heated up and kept at 160ºC for 6 hours. After the reaction product was cooled to room temperature, 100mL of a NaOH aqueous solution (50mg mL^{-1}), and acetone (350 mL) were added to it. Then, the mixture was stirred for few minutes and left overnight in the fridge. After that, the

precipitate was collected, dispersed in 60mL of deionized water, precipitated with 240mL of EtOH, and centrifuged (7800rpm, 10min). This step procedure was repeated four times. The remaining precipitate was dried overnight at 105^{o}C.

3.1.3 Electrode Preparation

Catalyst materials were supported on carbon black in order to achieve a 50wt% mass composition. Typically, 50mg of dried catalyst material was added to 10mL of deionized water and sonicated for 30min. After that, 50mg of carbon black and 2mL of ethanol were added to the suspension and sonicated for 1h. Lastly, the mixture was rota-evaporated at 70C and dried at 105°C for additional 12h. Catalyst inks were prepared as follows: 985µL of water, 985µL of ethanol and 30µl of Nafion were added to 5 mg of catalyst supported material. This ink mixture was sonicated for 2h and stored in the fridge. Prior to each electrochemical testing, inks were sonicated for 10min and glass carbon electrode (GCE) was cleaned with alumina, acetone, ethanol and water. Then, 20µL of ink was drop-casted onto the electrode surface (Area=0.196cm^2), and left to dry under air for about 30min.

3.1.4 Electrochemical measurements

All electrochemical measurements were conducted with a standard three-electrode cell system controlled by an Autolab PGSTAT30n potentiostat/galvanostat workstation equipped with a rotating disk electrode apparatus (RDE, PINE Research Instrument). Catalyst-modified GCE was used as working electrode, a platinum plate and

Hg/HgO (1M NaOH) as the counter electrode and reference electrode, respectively. All reported potentials were referred to reversible hydrogen electrode (RHE). To this end, the Hg/HgO (1M NaOH) reference electrode was calibrated with respect to RHE in H_2 saturated 1.0 M KOH electrolyte with a Pt electrode as the working electrode. This calibration gives rise to E(RHE)=E(Hg/HgO (1M NaOH)) + 0.93 V. All electrocatalytic measurements were acquired in an O_2-saturated aqueous 1M KOH electrolyte using the RDE, which was continuously rotated at 1600 rpm to get rid of oxygen bubbles during experiments. Linear sweep voltammetry (LSV) was carried out at 5 mV s^{-1} for the OER polarization curves. Tafel slope was derived from these polarization curves. Prior to measuring polarization curves, catalysts were cycled 4 times by cyclic voltammetry (CV) at 50 mV s^{-1} to develop a stable CV curve. All polarization curves were corrected with 85% iR-compensation. Catalyst stability performance was evaluated by two methods: 1) Chronopotentiometry was carried out under a constant current density of 10 mA cm^{-2} with the catalyst loaded on GCE as working electrode; 2) Accelerated cycling test at which LSV curves were obtained before and after 3000 CV cycles between 1.1 and 1.6 V (vs RHE) at 50mV s^{-1}. The electrical double-layer capacitance (Cdl) of all samples was determined by CV recorded in a potential range of 1.1 V and 1.2 V vs. RHE from 10 to 120 mV s^{-1}. The plot of current against scan rate was taken at 1.15 V vs. RHE, which display a linear fit and the slope corresponds to the double layer capacitance (Cdl). Electrochemical impedance spectroscopy (EIS) measurements were carried out for all the catalysts at 1.53V (versus RHE) over a frequency range from 100 kHz to 0.1 Hz with a 5 mV AC dither.

3.1.5 Turnover Frequency (TOF) Calculation

The TOF values were calculated using the following equation[64] :

$$TOF = \frac{J * A}{4 * F * m}$$

Where J is the current density at a given overpotential in A cm $^{-2}$, A is the geometric area of working electrode, F is the faraday constant (96485 C mol^{-1}) and *m* is the total number of moles of Ni+Fe deposited on the working electrode.

The current density used for TOF calculation was obtained from polarization curves measured at a scan rate of 1 mV s $^{-1}$ and 85%iR corrected before TOFs estimation. All the Ni and Fe atoms were regarded as the active sites in order to give a more conservative estimation of TOF.

3.1.6 Material Characterization

Scanning transmission electron microscopy and transmission electron microscopy (STEM and TEM) images were obtained for the as-prepared electrocatalyts using a Scanning Transmission Electron Microscope Hitachi HD2700C operated at 200 kV, equipped with both High-Angle Annular Dark Field and energy-dispersive X-ray spectroscopy **(**EDS**)** detectors. Samples were prepared by in isopropyl alcohol, sonicated for 5min, and then drop casted onto honey carbon coated copper grids. The samples were air-dried prior to analysis. The total metal content of the catalysts was measured by inductively coupled plasma optical emission spectrometry (ICO-OES) using a Spectro Arcos ICP OES instrument. Samples were prepared by dissolving ∼10 mg of catalysts in

2mL of aqua regia (75vol% HCl and 25vol% HNO_3) at 120°C for 2h. The resulted solution was diluted to 10mL with deionized water and then analyzed using ICP-OES. C, H and N elemental analysis of all catalysts were performed using a Perking Elmer 2400 series II equipment. X-ray diffractograms were obtained using a Maxima Shimadzu equipment with a standard Cr/ Co/Cu ceramic sealed tube (λ= 0.154060 nm) operated at 40kV and 30mA. X-ray photoelectron spectroscopy (AP-XPS) measurements were performed using a commercial SPECS AP-XPS chamber equipped with a PHOIBOS 150 EP MCD-9 analyzer and Al Kα source (E = 1486.6 eV) at the Chemistry Department of Brookhaven National Laboratory (BNL) (resolution: ~0.2 eV). The C1s photoemission line was used for the energy calibration. Powder samples were loaded on a copper tape and then inserted into the XPS ultra-high vacuum chamber.

3.2 Co and Ni-ZnO catalysts for CO_2 Hydrogenation

3.2.1 Materials

Ammonium Hydroxide (NH_4OH, 35%), Ethanol (EtOH, 99%), Urea (99%) and Acetone (99%) were purchased from Synth, Brazil. Nickel(II) nitrate hexahydrate ($NiNO_3$. $6H_2O$, 99%), Cobalt (II) nitrate hexahydrate ($CoNO_3$. $6H_2O$, 98%), Zinc(II) nitrate hexahydrate ($ZnNO_3$. $6H_2O$, 98%), Cobalt(III) oxide (Co_2O_3, 98%), Cobalt(II,III) oxide (Co_3O_4, 99%), Titanium oxide (TiO_2, 98% anatase phase), Ceria oxide (CeO_2, 99%), Zin oxide (ZnO, 98%), and Sodium hydroxide (NaOH, 98%) were purchased from Sigma-Aldrich. All materials were used as received without any further purification.

3.2.2 Catalyst preparation

Zinc oxide (ZnO) was synthesized by a precipitation method. In a typical synthesis, 20 g of $Zn(NO_3)_2$ was dissolved in 2000 mL of distilled water under constant stirring. Then, 600 mL of an NH_4OH solution (0.15 mol L^{-1}) was added into the reaction mixture producing a white suspension. Afterward, 25ml of NaOH (1mol L^{-1}) were added to produce a flake-like white precipitate. The resulting mixture was further stirred for 10min and the solid was decanted overnight. The precipitate was concentrated, washed with water (400mL) and ethanol (200mL) to obtain a white solid product, and finally dried at 80°C overnight. The series of nickel/zinc oxide (Ni/ZnO) and cobalt/zinc oxide (Co/ZnO) catalysts with different metal loadings were prepared by incipient wetness impregnation. Typically, the intended amount of cobalt(II) or nickel (II) nitrate hexahydrate ($Co(NO_3)_2{\cdot}6H_2O$ and $Ni(NO_3)_2{\cdot}6H_2O$, respectively, was first dissolved in deionized water at room temperature, and the solution was dropwise added to the as-prepared ZnO support for impregnation. The mixed slurries were then aged at room temperature for 12 h and dried overnight at 120 °C. The resulting products were finally calcined in air at 400 °C (5 °C/min) for 6 h using a tubular furnace. The obtained catalysts were denoted as x% Ni/ZnO or x% Co/ZnO in which x refers to the weight percentage metal loading.

3.2.3 Catalytic performance evaluation

The evaluation of the CO_2 hydrogenation activity for the Ni/ZnO and Co/ZnO catalysts was carried out using a flow fixed-bed quartz tube reactor with an inner

diameter of 4 mm under atmospheric pressure. About 20 mg of catalyst was mixed with ~20 mg of inert material (acid-purified quartz which was pre-calcined at 900 °C for 2 h, 60−80 mesh) packed into the reactor and supported by quartz wool. Catalyst materials were not sieved for particle size. Prior to reaction, the catalysts were pre-treated in H_2 (10 mL/min) at 400°C (heating rate from RT of 10°C/min) for 1 h, cooled to room temperature, and then exposed to the CO2 hydrogenation reaction conditions. The ratio of reactant gases was set at 1:5 (2.5 mL/min CO_2 and 12.5 mL/min H_2, respectively) and diluted by N2 (10 mL/min) which was used as an internal standard. For the catalytic performance evaluation, the catalysts were heated to 150°C with a 10°C/min ramping, and measurements were taken in 100°C increments up to 450°C. At each temperature step, which took 1h, three data points were taken. The concentrations of effluent gas products were monitored by a gas chromatography instrument (Agilent 7890B) equipped with both flame ionization and thermal conductivity detectors.

In this study, the conversion of CO_2 is defined as

$$Conversion\ (CO_2)\% = \left(1 - \frac{CO_2 out}{CO_2 in}\right) * 100\%$$

The activity is defined as

$$Activity\ (product)\left[\frac{\mu mol}{g_{metal}\ h}\right] = \frac{P_{product} * flow\ rate}{1.344 *\ m_{metal}}$$

The selectivity of CO and CH_4 are defined, respectively, as

$$Selectivity\ (CO)\% = \left(\frac{P_{CO}}{P_{CO} + P_{CH_4}}\right) * 100\%$$

$$Selectivity\ (CH_4)\% = \left(\frac{P_{CH_4}}{P_{CO} + P_{CH_4}}\right) * 100\%$$

3.2.4 Characterization of catalysts

High-resolution transmission electron microscopy (HR-TEM) images were obtained for the as-prepared 1.9wt% Ni, 7.7%wt Ni, 3.3%wt Co, and 9.7%wt Ni/ZnO and Co/ZnO using a JEOL JEM 2100 equipped with a field emission electron source and operated at 200 kV. Samples were dispersed as a suspension in isopropyl alcohol, sonicated for 5min, and then drop casted onto a honey carbon coated copper grid. The samples were air-dried prior to analysis. The diffratogram patterns of catalysts were collected at the 17BM beamline (λ = 0.24125 Å) of the Advanced Photon Source (APS) at Argonne National Laboratory (ANL). The total cobalt and nickel loading supported on the catalysts were determined by Flame atomic absorption spectroscopy (FAAS) using a Shimadzu AA-6300 spectrophotometer equipped with an Ni and Co hollow cathode lamps (Photron). Samples were prepared by dissolving ∼15 mg of catalysts in 2mL of aqua regia (75vol% HCl and 25vol% HNO_3) at 120°C for 2h. The resulted solution was diluted to 10mL with deionized water and then analyzed using FAAS.

3.2.5 *In situ* Ambient Pressure X-ray Photoelectron Spectroscopy (AP-XPS)

Ambient Pressure X-ray photoelectron spectroscopy (AP-XPS) measurements were performed using a commercial SPECS AP-XPS chamber equipped with a PHOIBOS 150 EP MCD-9 analyzer and Al Kα source (E = 1486.6 eV) at the Chemistry Department of Brookhaven National Laboratory (BNL) (resolution: ∼0.2 eV). The C1s or Zn2p photoemission line was used for the energy calibration. Powder samples (1.9 wt% Ni, 7.7 wt% Ni, 3.3 wt% Co, and 9.7 wt% Co/ZnO as-prepared catalysts) were pressed on an

aluminum plate and then loaded into the AP-XPS ultra-high vacuum chamber. A 20 mTorr atmosphere pressure of H_2 was used to pretreat the sample at 400°C for 0.5 h before a reaction mixture of 5 mTorr of CO_2 and 25 mTorr of H_2 was introduced into the reaction chamber through a high precision leak valve. O 1s, C 1s, Co 2p, Ni 2p, Zn 2p, and Zn LMM XPS regions were collected at 25 °C before pretreatment, at 25 °C after reduction, and at different temperatures (25, 250, 350, and 450 °C) under a reaction gas environment.

3.2.6 *In Situ* Time-Resolved X-Ray Diffraction (XRD)

The in situ time-resolved XRD measurements on 1.9 wt% Ni/ZnO under the RWGS reaction was performed at the 28ID XPD beamline (λ = 0.24172 Å) of the National Synchrotron Light Source II (NSLS II) at Brookhaven National Laboratory (BNL). Typically, 3 mg of the powder sample was loaded into a 1.0 mm diameter amorphous silica tube. This was connected to an in situ gas flow reactor equipped with a resistance heater placed under the silica tube. The sample was then pretreated in H_2 (6ml/min) at 400 °C (30min, ramping rate of 20 °C/min) and its structural transformation was monitored by XRD. After that, the XRD measurements under RWGS reaction conditions were performed ranging from room temperature up to 450 °C with a 20 °C/min ramping rate and a time span of 30 min at each temperature stage (RT, 150, 250, 350 and 450°C). The Two-dimensional XRD patterns were collected continuously with a PerkinElmer amorphous silicon detector during reaction.

4. RESULTS AND DISCUSSION

4.1 NiFe-electrocatalysts for Oxygen Evolution Reaction

Different from typically reported protocols, we prepared our catalyst materials by mixing precursors of metal and carbon sources (citric acid and urea), which resulted in both Ni-Fe$(OH)_2$ and carbon nanostructures being formed *in situ* and blended together. The crystalline structure of the pristine Ni, Fe and mixed Ni−Fe catalysts was assessed by X-ray diffraction (XRD). As shown in **figure 5**, all Ni-containing catalysts show broad diffraction peaks located at around 11°, 22°, 34°, 39°, and 60° which can be assigned to the (003), (006), (101) and (110) lattice planes of layered α-Ni$(OH)_2$ (pdf # 00-038-0715), respectively.[63,96] It is noteworthy that upon increasing Fe content, the diffraction patterns of Ni-Fe oxyhydroxides become relatively lower in intensity and slightly shift to higher angles in comparison with pristine α-Ni$(OH)_2$, in particular for the (003) reflection. These observations are in line with previous reports in which Fe intrusion in Ni lattices can induce the formation of more distorted phase as well as lattice shrinkage. [22,24,29,63] The Fe catalyst showed reflections with low intensity at positions, 32°, 35°, 41°, and 63° 2θ, which can be ascribed to ferrihydrite structures.[97,98]

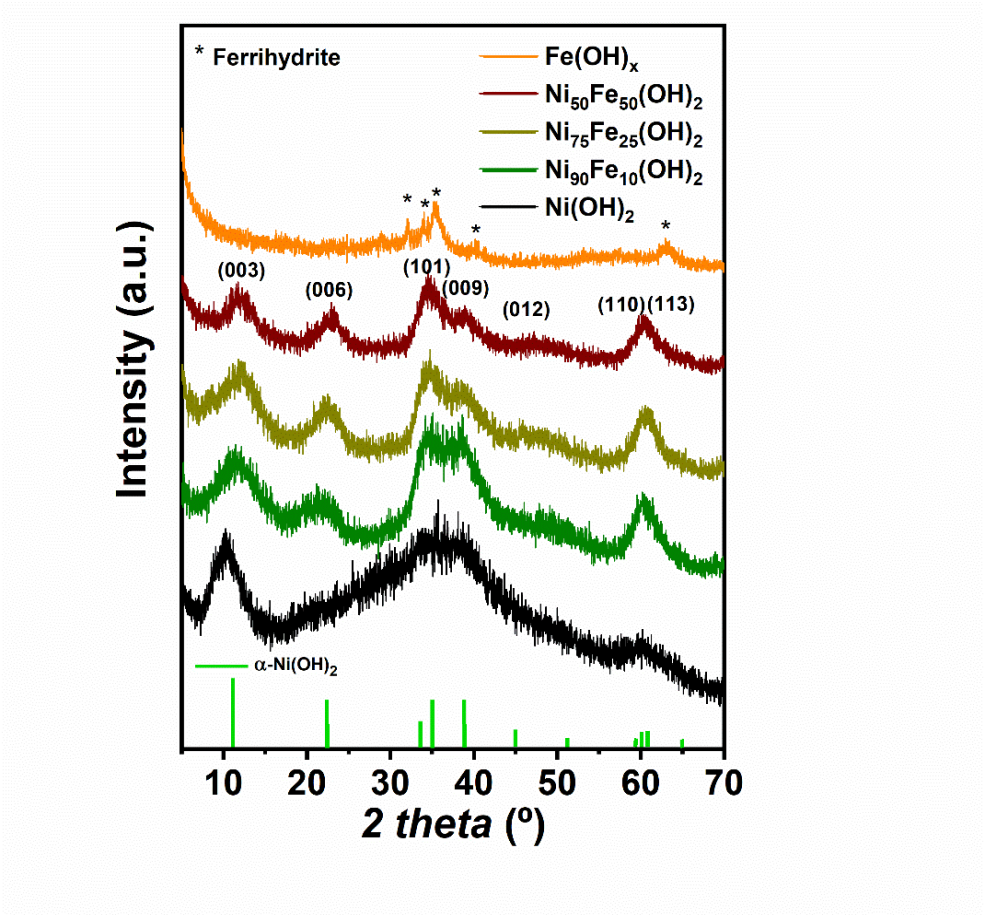

Figure 5. Powder XRD pattern of as-made Ni−Fe catalysts with different Ni:Fe ratio compositions ($Ni_{100-x}Fe_x(OH)_2$).

Bright and dark field transmission electron microscopy (TEM) images (**figure 1a** and **2b**, respectively) of the $Ni_{75}Fe_{25}(OH)_2$ catalyst as a representative example suggest that its morphology predominantly consists of an assembly of many nanosheets. High-angle annular dark-field scanning transmission electron microscopy (HAADF−STEM) image (**figure 6c**) and the corresponding energy-dispersive X-ray spectroscopy (STEM-EDS) mappings (**Figures 6d-i**) show that both Ni and Fe as well as C, N, O and Na are homogenously distributed across the sample, indicating that the Ni-Fe hydroxide phase is well associated with a carbon nanostructure without any significant compositional segregation.

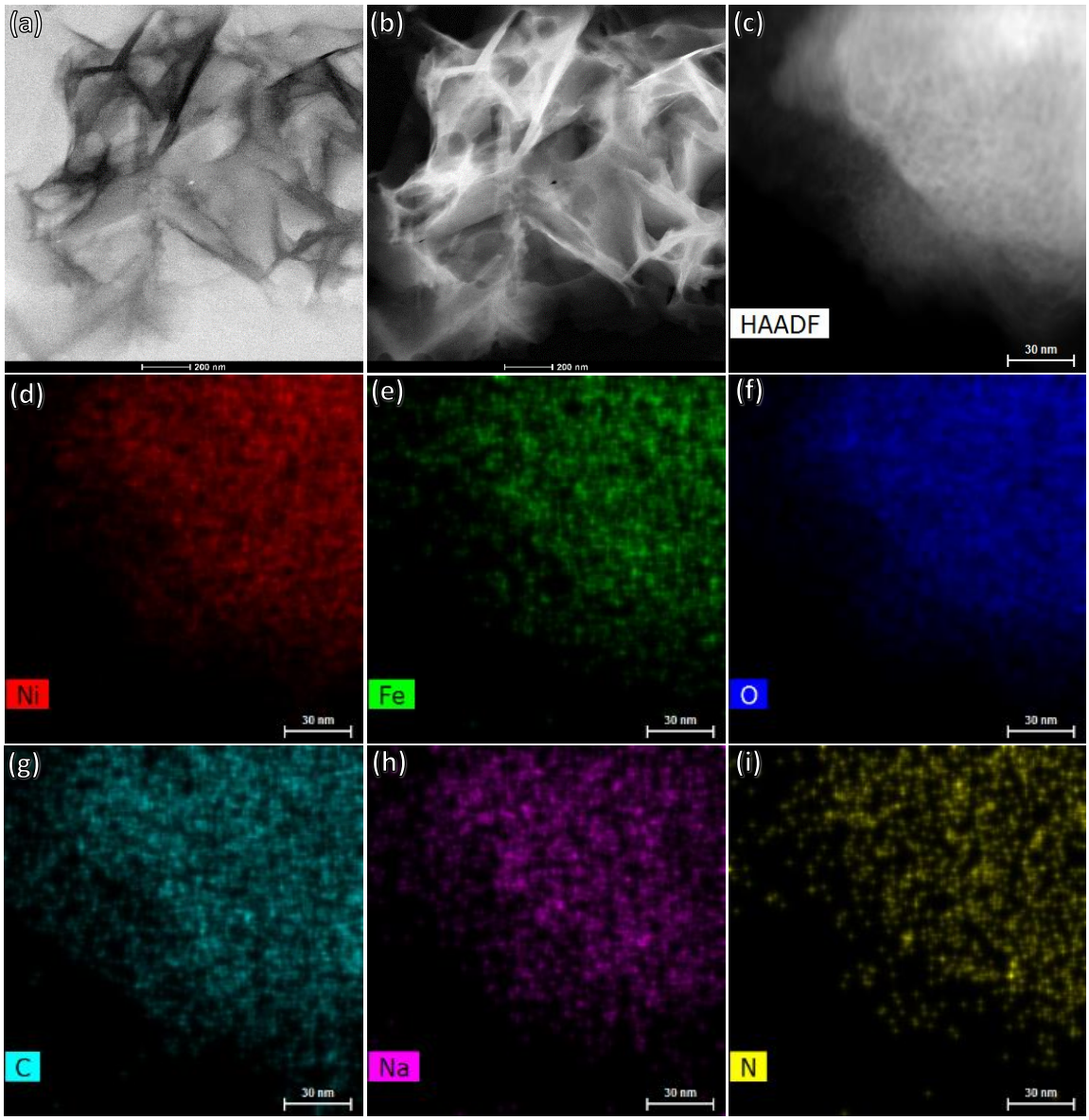

Figure 6. Bright (a) and dark field (g) transmission electron microscopy (TEM) images, STEm-HAADF image (c), and STEM-EDX elemental maps for Ni (d), Fe (e), O (f), C (g), Na (h), and N (i) in the $Ni_{75}Fe_{25}(OH)_2$ catalyst.

In order to evaluate the electrocatalytic oxygen evolution (OER) activities of the $Ni_xFe_{100-x}(OH)_2$ catalysts, electrochemical measurements were carried out in O_2 saturated 1M KOH solution using 50wt% carbon black (Vulcan XC72R ("C")) supported catalysts, which were previously drop-casted on GCE electrodes with a constant mass

loading of ~0.25mg cm^{-2}. **Figure 7a** depicts iR-corrected OER LSV curves of the samples. Notably, all Ni-based (oxy)hydroxide catalysts show the Ni^{2+}/Ni^{3+} oxidation wave in the potential range of 1.34–1.44 V (vs reversible hydrogen electrode (RHE)), which shifts to higher potentials as the Fe content increases. This behavior is generally attributed to strong electronic interaction between Ni and Fe and is also considered to be an indicative of Fe incorporation into the $Ni(OH)_2$ structure.[22,24,29] Regarding the OER activity (**figure 7a**), all Ni-Fe mixed catalysts showed enhanced OER catalytic activity to achieve a geometric current density of 10 mA cm^{-2} when compared to the pristine $Ni(OH)_2$/C, Fe(OH)x/C, and even the state-of-the-art Ir/C catalyst (**figure 7b**). This result suggests a synergism between Ni and Fe centers in agreement with previous studies.[22,24,29,63] Among the Fe-doped Ni-based catalysts, $Ni_{75}Fe_{25}(OH)_2$/C exhibited the best OER performance with low overpotential of 234±2mV and 279±13 mV to achieve 10 and 100 mA cm^{-2} current density, respectively. To the best our knowledge, this OER performance is on a par with most of the best non-noble metal containing OER catalysts reported to date, which is illustrated in **table 1**. [24,29,63,64]

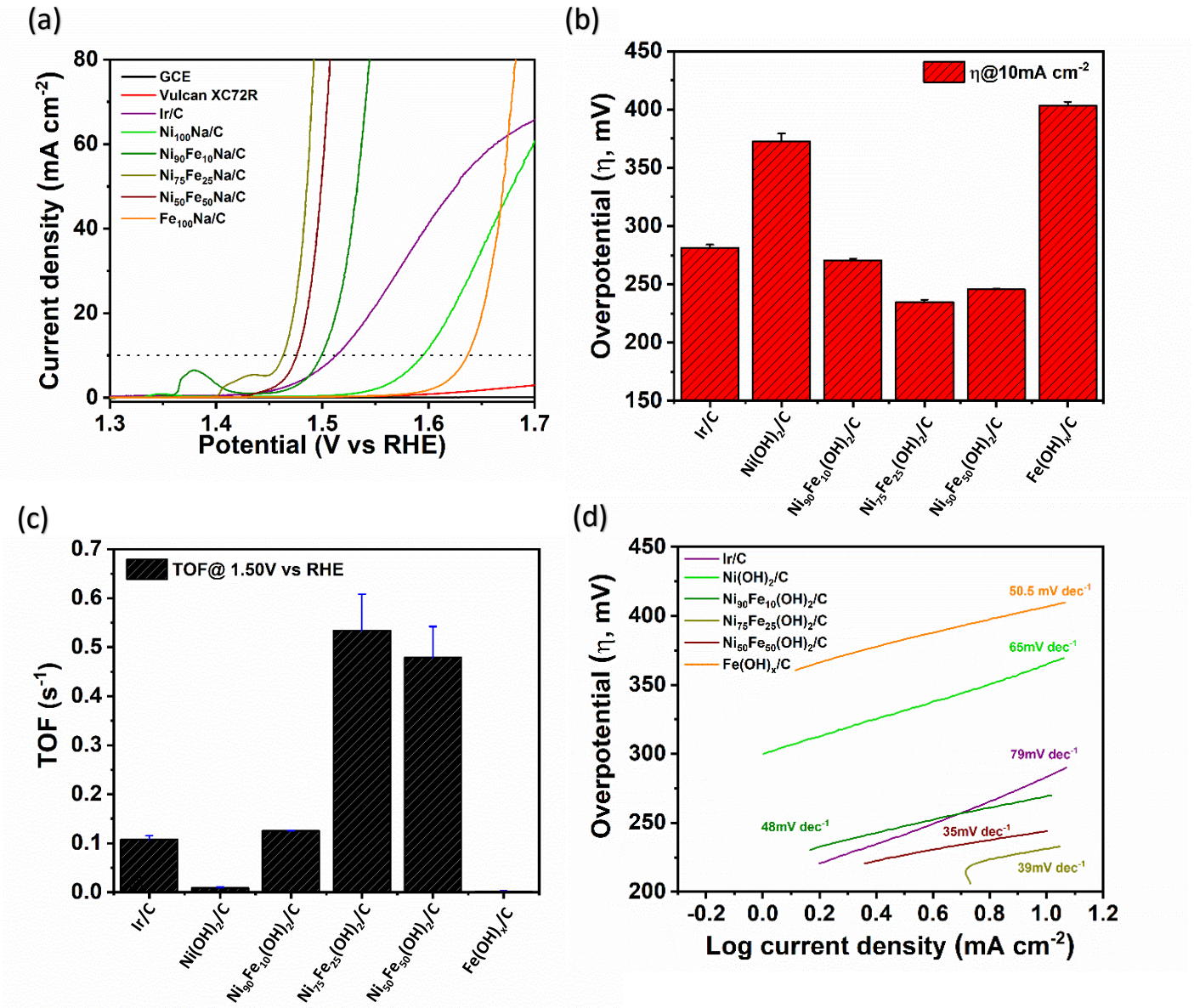

Figure 7. (a) OER LSV curves of the carbon supported ("/C") $Ni(OH)_2$, $Fe(OH)_x$ and Ni–Fe oxyhydride catalysts performed at scan rate of 5 mV s^{-1} (b) OER activity summary of catalysts quantified as overpotential required to achieve 10 mA cm^{-2} on a geometric basis (Overpotential = E(V) at 10mA cm^{-2} - 1.23V). (c) Turnover frequency (TOF) on the basis of the total metal loading of Ni+Fe (determined by ICP-OES), estimated at η = 270 mV from polarization curves measured at 1 mV/s. (d) Tafel plots. All LSV curves were carried out in O_2 saturated 1 M KOH solution at 1600rpm and with 85% iR-compensation.

Table 1. Comparison of OER performance of electrocatalysts from recent publications.

Catalyst	Substrate	Catalyst loading (mg cm^{-2})	Electrolyte	Overpotential (mV) j=10 mA cm^{-2}	Tafel slope (mV dec^{-1})	Ref.
$Ni_{0.83}Fe_{0.17}(OH)_2$	GCE[a)]	0.20	1 M KOH	245	61	[29]
NiFe/RGO	GCE	1.0	1 M KOH	245	-	[99]
NiFe LDH-NS@DG	GCE	0.28	1 M KOH	210	52	[100]
FeNi LDH	NF[b)]	0.25	1 M KOH	232	48	[101]
NiFe LDH exfoliated[j)]	GCE	0.07	1 M KOH	302	40	[102]
NiFe LDH/CNT hybrid	CFP[c)]	0.25	1 M KOH	247	31	[103]
NiFe LDH-MoO_4^{2-}	GCE	0.28	1 M KOH	280	40	[104]
FeNi-rGO LDH hybrid	NF	0.25	1 M KOH	206	39	[101]
NiFe LDH	GCE	0.07	1 M KOH	347	67	[102]
Fe^{2+} -NiFe LDH colloid	GCE	0.20	1 M KOH	249	35	[59]
$Ni_{75}Fe_{25}(OH)_2$/C	GCE	0.25	1 M KOH	234	39	**This work**

a) Glass carbon electrode; b) Nickel foam; c) Carbon fiber paper; rGO - reduced graphene oxide; CNT – Carbon nanotubes.

In the context of the OER, TOF is defined as the number of O_2 molecules a catalytic site evolves per unit of time.[17] In general, it is regarded as an important activity metric to quantitatively compare different OER catalyst materials.[17,59,105] Thus, in order to gain more insights into the intrinsic catalytic OER activity of our catalysts, turnover frequencies (TOFs) were determined. The total metal content (Ni+Fe) displayed in **table**

2 was assumed to be equal to the number of active sites in the electrocatalysts. As shown in **figure 7c**, $Ni_{75}Fe_{25}(OH)_2$ /C displays the highest TOF values among the samples ($0.53 \pm 0.07 s^{-1}$ and $1.15 \pm 0.07 s^{-1}$ at $\eta = 270$ and 300 mV, respectively). These values appear to be among the best TOFs for reported mixed Ni–Fe-based catalysts.[24,59,63,64] However, a more detailed and direct comparison between these values and those in previous works is quite challenging due to some differences in reaction conditions, catalyst loadings, and methods for the quantification active sites.[24,63,64] **Figure 7d** summarizes the Tafel slope for all catalysts. $Ni_{75}Fe_{25}(OH)_2$ /C (39 mV dec^{-1}) shows a similar Tafel slope to that of $Ni_{50}Fe_{50}(OH)_2$ /C (35 mV dec^{-1}), but this was considerably smaller than the other catalysts. This small Tafel slope associated with the apparently good TOF value suggests that the Ni/Fe ratio in $Ni_{75}Fe_{25}(OH)_2$ /C offers the most synergism between Ni and Fe, which facilitates the kinetics of OER and enhancing intrinsic activity.

To further understand the catalytic behavior of our electrocatalysts, we estimated the double-layer capacitance (C_{dl}) and measured the electrochemical impedance spectroscopy (EIS) of all materials. In general, the C_{dl} is used to roughly represent the corresponding electrochemical active surface area (ECSA) of the samples.[29,64] As shown in **figure 8a**, C_{dl} values suggests that $Ni_{75}Fe_{25}(OH)_2$ /C possesses a relatively high ECSA among its counterparts, which could be one of the reasons for its superior OER catalytic activity. However, further studies are still required for a proper assessment of the ECSA. It is noteworthy that C_{dl} values may become an unreliable indicator for ECSA due to variations in the electrical conductivity of catalysts.[10] Regarding EIS analysis, small semicircles are mainly associated with decreased charge-transfer resistances (Rct), which in turn result in considerably accelerated reaction

kinetics.[23,29,64,106] Notably, the Nyquist plots (**figure 8b**) show that $Ni_{75}Fe_{25}(OH)_2$ /C displays the smallest semicircle among the tested catalyst materials, thus indicating a significantly lower Rct. Interestingly, the Rct order matches perfectly with the trend in the OER activity for the different catalysts. This suggests that the excellent charge-transfer capability of $Ni_{75}Fe_{25}(OH)_2$ /C can be regarded as a crucial parameter to its superior intrinsic OER activity.

Table 2. Bulk composition of the unsupported Ni-Fe catalysts.

	Ni_{100}	**$Ni_{90}Fe_{10}$**	**$Ni_{75}Fe_{25}$**	**$Ni_{50}Fe_{50}$**	**Fe_{100}**
Ni/Fe in precursor	100/0	90/10	75/25	50/50	0/100
Bulk Ni/Fe [a)]	100/-	91/9	77/23	57/43	-/100
Ni [wt%][a)]	20.7±1.5	35.2±1.8	33.1±0.6	28.0±0.9	-
Fe [wt%][a)]	-	3.5±0.1	9.8±0.2	20.6±0.7	48.7±0.7
Ni+Fe [wt%][a)]	20.7	38.7	42.9	48.7	48.7
Bulk C [wt%][b)]	15.6±0.2	10.4±0.1	9.4±0.3	7.2±0.1	3.9±0.1
Bulk H [wt%][b)]	2.1±0.1	2.7±0.1	2.8±0.1	2.6±0.1	1.6±0.1
Bulk N [wt%][b)]	1.2±0.1	0.9±0.2	0.4±0.1	0.3±0.1	0.3±0.1

a) Mole ratio and total weight percentage [wt%] of metal were determined by ICP-OES;
b) weight percentage [wt%] of C, H and N were obtained by elemental analysis.

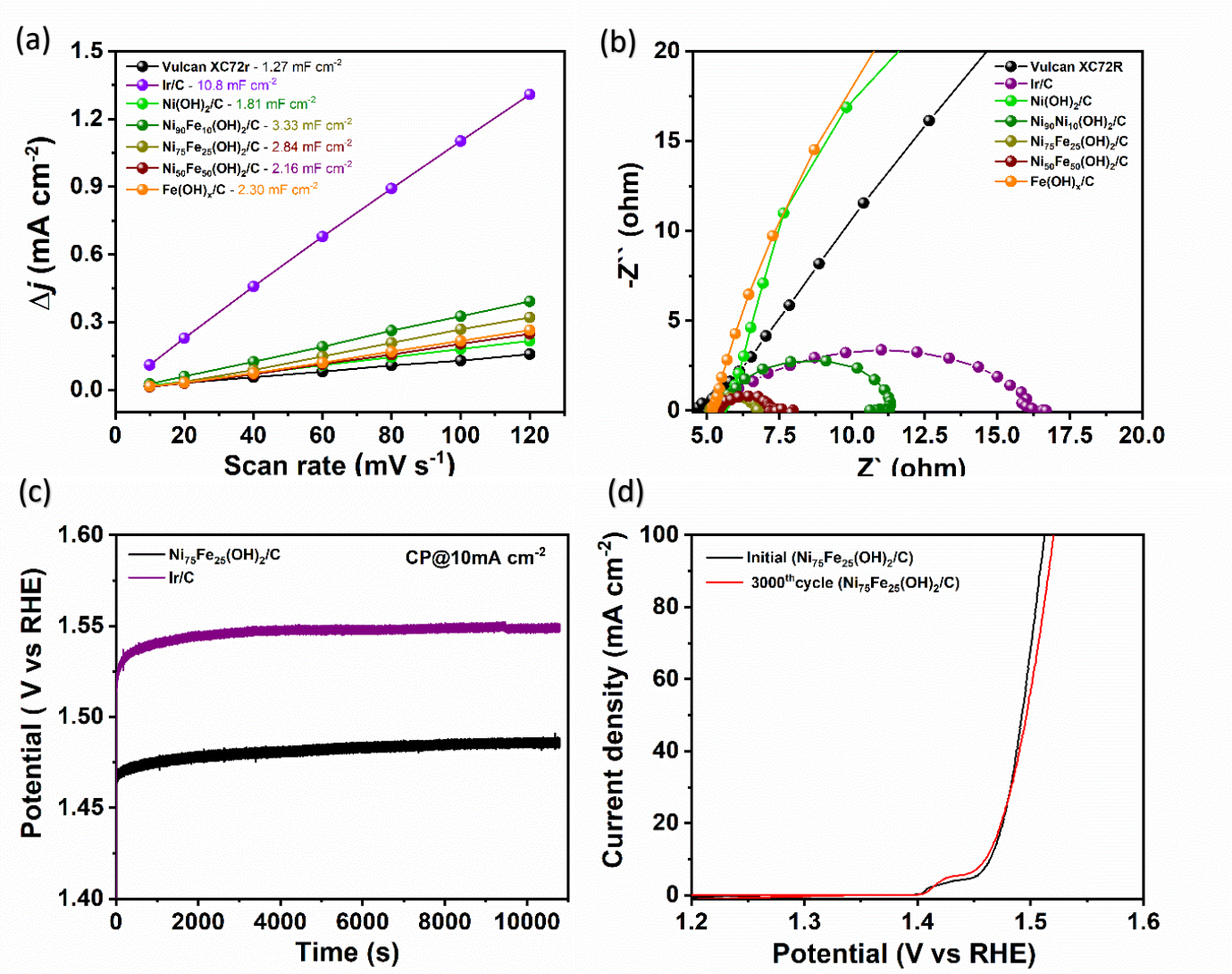

Figure 8. (a) Double layer capacitance (Cdl) at 1.15 V (vs. RHE) derived from CVs recorded between 1.1 to 1.2V (vs RHE) at different scan rates, i.e. 10, 20, 30, 40, 60, 80, 100 and 120mV s^{-1}. (b) EIS of the carbon supported Ni-Fe catalysts at 1.53V (versus RHE) over a frequency range from 100 kHz to 0.1 Hz with a 5 mV AC dither. (c) Catalyst stability: chronopotentiometry curve of $Ni_{75}Fe_{25}(OH)_2$/C at 10 mA cm^{-2} and 1600 rpm. (d) Stability test: LSV curves (85% iR-compensation) for the $Ni_{75}Fe_{25}(OH)_2$/C catalyst before and after 3000 CV cycles between 1.1 and 1.6 V (vs RHE) at 50mV s^{-1}. All experiments were performed in O_2 saturated 1M KOH.

In addition to catalytic activity, we investigated the stability of $Ni_{75}Fe_{25}(OH)_2$ /C by both long-term chronopotentiometry and repeated cyclic voltammetry scanning experiments. As displayed in **figure 8c**, $Ni_{75}Fe_{25}(OH)_2$ /C can maintain a current density of 10 mA cm^{-2} with only ~15 mV overpotential increase even after after 3 h. This slight activity loss is significantly less than what was observed for Ir/C, which showed a ~30mV overpotential increase under the same testing conditions. Additionally, after 3000 CV cycles, the $Ni_{75}Fe_{25}(OH)_2$ /C initial and final OER polarization curves (**figure 8d**) revealed no significant loss in catalytic current, further confirming the good stability of the catalyst material even under accelerated reaction conditions.

X-ray photoelectron spectroscopy (XPS) studies were performed to assess the surface composition as well as the chemical state of the metals in our catalyst materials. As shown in **figure 9a**, all Ni-based oxyhydroxides exhibit two fitting peaks at around 856 eV and 873 eV with their corresponding satellite peaks (denoted as sat.). Namely, these binding energies (BE) values can be assigned to the Ni $2p_{3/2}$ and Ni $2p_{1/2}$ spin–orbit peaks of Ni^{2+} oxidation state, respectively.[29,59,64] Another interesting feature from the XPS analysis is depicted in **figure 9b**. Noticeably, a significant C 1s region can be ascribed to all as-prepared catalyst materials. Likewise, elemental analysis confirms that carbon is present in the bulk composition of all samples, which is ~10wt% for $Ni_{75}Fe_{25}(OH)_2$ (**table 2**). These results corroborate with those of HAADF-STEM mappings and suggest that a carbon structure, apart from the support, is integrated to the (oxy)hydroxides. This *in situ* formed carbon structure may play an important role in the observed OER activity of our catalyst system. Particularly, as it can benefit the composite electrocatalyst materials enhancing their conductivity and exposing more surface catalytic active sites for the OER.[64] Even though nitrogen was also detected using

HAADF-STEM mappings and elemental analysis (**table 2**), its bulk quantity is quite small and thus its impact on the OER performance of our catalyst materials should not be significative.

In the Fe 2p region (**figure 9c**), $Ni_{75}Fe_{25}(OH)_2$ catalyst show clearly the Fe $2p_{3/2}$ core level signal. It worthy note that by further deconvolution of the Fe $2p_{3/2}$ peak, Fe^{2+} $2p_{3/2}$ (709.2 eV) and Fe^{3+} $2p_{3/2}$ (711.5 eV) signals could be assigned to this catalyst.[29,106] These observations suggest the presence of the Fe^{2+} dopant in the $Ni_{75}Fe_{25}(OH)_2$ material. This may play an important role in the superior catalytic activity displayed by it. In particular, since previous reports have shown that Fe^{2+}/Fe^{3+}- Ni catalysts are generally more active for the OER than the ones containing only Fe^{3+}.[59] In fact, introducing Fe^{2+} into NiFe-LDH was suggested by the authors to promote a redox behavior difference in Fe^{2+}-O-Fe^{3+} motifs with respect to isolated Fe^{3+} under OER working condition. Specifically, high-valence $Fe^{(3+\delta)+}$ species are formed for the motifs, which are slightly stable even when the potential gets back to 0 V, whereas no significant valence state higher than +3 is observed for isolated Fe^{3+} centers. This modulation in the local electronic structure within the LDH structure under reaction conditions was pointed out as a main reason for enhancement in OER activity. This is in agreement with recent studies that have suggested that high-valent metal species (e.g. Fe^{4+}) are the likely OER active site in NiFe systems.[105,107,108] More specifically, it has been suggested that such high-valent states contribute to modulate the OH - $M^{(2+\delta)}$ bond strength of the OH intermediate with respect to the $M^{(2+\delta)}$ center, facilitating an increase of the overall rate of oxygen evolution. [17,28]

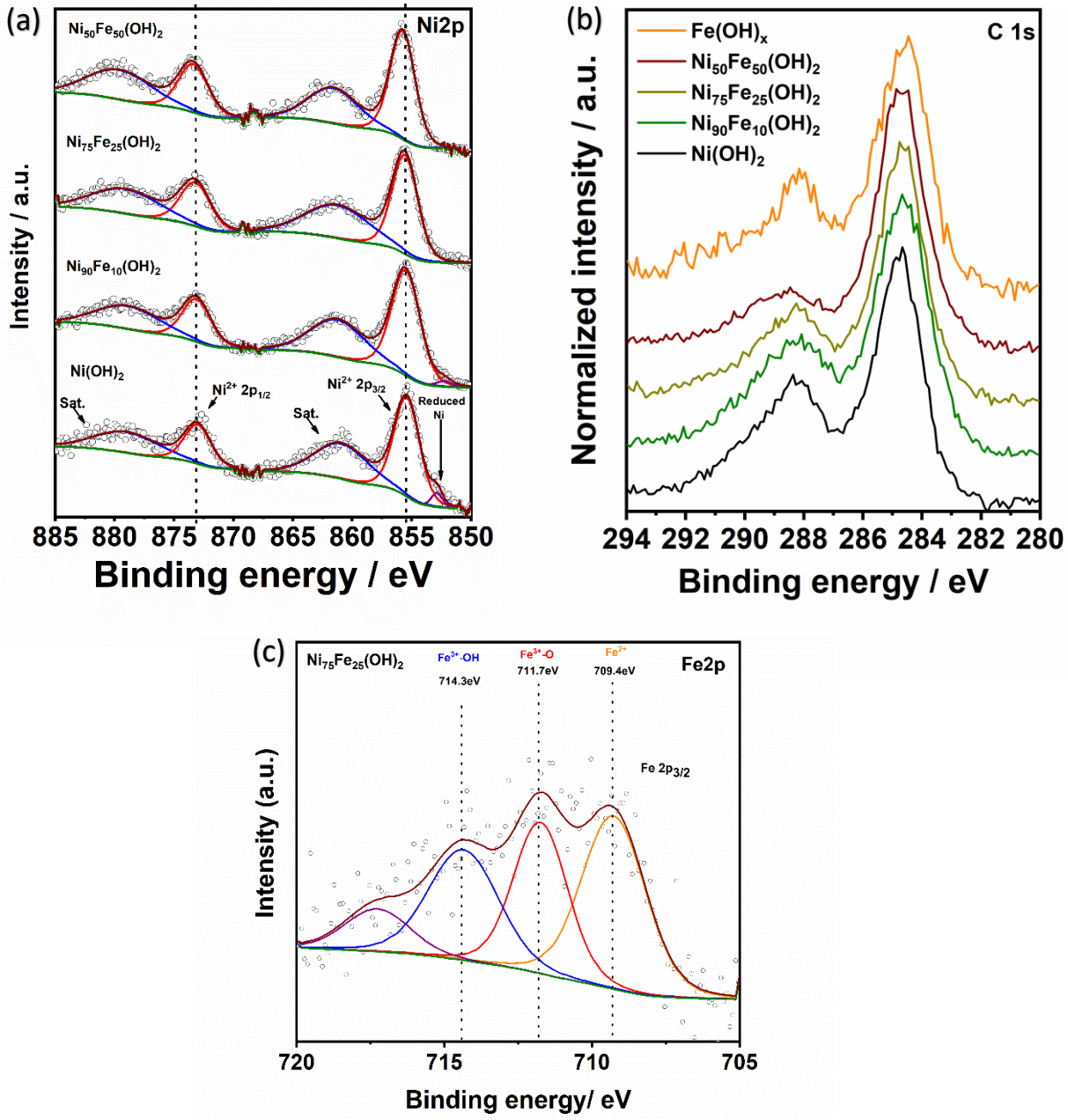

Figure 9. High-resolution X-ray Photoelectron Spectroscopy (XPS) spectra of the as-prepared catalysts. (a) Ni 2p XPS spectra for $Ni_{50}Fe_{50}(OH)_2$, $Ni_{75}Fe_{25}(OH)_2$, $Ni_{90}Fe_{10}(OH)_2$, and pure $Ni(OH)_2$. (b) Fe 2p XPS spectra for $Ni_{50}Fe_{50}(OH)_2$, $Ni_{75}Fe_{25}(OH)_2$, and $Ni_{90}Fe_{10}(OH)_2$. (c) C1s XPS spectra for all catalysts. Binding Energy (BE) shifts are indicated by the dashed lines shown in (a) and (b).

4.2 Co/ZnO and Ni/ZnO catalysts for CO_2 Hydrogenation

The crystalline structure of the as-prepared "x"wt% Ni/ZnO and "x"wt% Co/ZnO catalysts was firstly assessed by X-ray diffraction (XRD) (where "x" refers to the metal loading). As shown in **figure 10a** and **10b**, the majority of the diffraction peaks come from the hexagonal wurtzite structure of pure ZnO (CIF - 1811117).[92,109] Nearly all Co-containing catalysts (**figure 10a**) show diffraction peaks located at around 2.9°, 4.8°, 5.8°, 6.8°, 8.4°, 8.9°, and 9.6° which can be assigned to the (111), $(10\bar{1})$, $(1\bar{1}1)$, (220), $(11\bar{2})$, (331), and $(20\bar{2})$ lattice planes of cubic Co_3O_4 (CIF - 18565), respectively.[110,111] XRD patterns for catalysts with various Ni loadings are provided in **Figure 10b**. As it can be observed, there are four diffraction patterns located at around 5.7°, 4.8°, 6.6°, 10.9°, and 11.3°, which could be indexed into the (010), (110), (120), and (200) lattice planes of NiO structure (CIF – 1819800), respectively.[92,109] It is noteworthy to highlight that signals from both Co_3O_4 and NiO phases were only clearly detected upon increasing metal content up to 4 wt% in both catalysts. Also, an increase in the intensity of the peaks took place with the metal loadings. The absence of some characteristic peaks of Co_3O_4 and NiO for the samples with the two lowest metal loadings can be ascribed to the poor crystallinity of both cobalt and nickel at such low loadings.[36,112] Furthermore, the sharp Co_3O_4 and NiO peaks in the highest metal loading catalysts indicate much larger average crystallite size of the Co and Ni oxide phases, implying the agglomeration of such phases during the synthesis process can occur.[112,113] In order to account for the formation of more distorted phase as well as any lattice shrinkage in the catalyts due to Ni and/or Co intrusion into ZnO lattices or vice-versa, further studies such as retvield refinement are currently being performed.

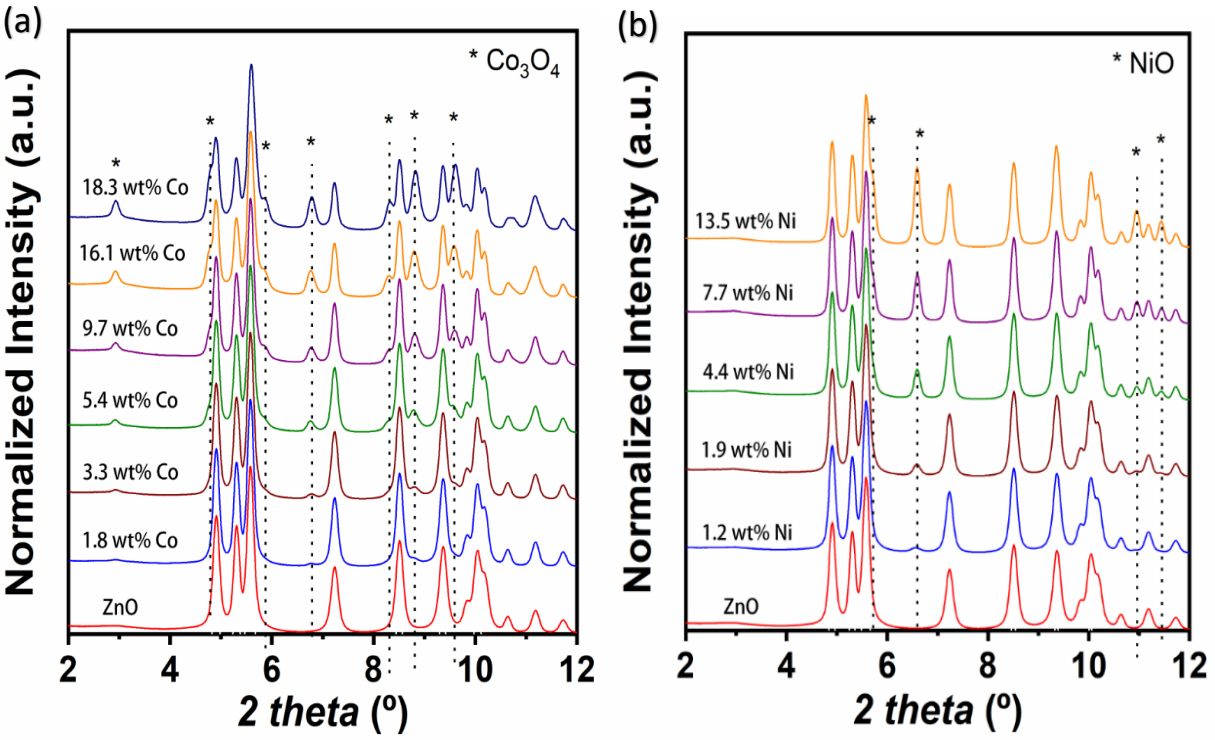

Figure 10. Ex-situ XRD patterns of fresh Co/ZnO (a) and Ni/ZnO (b) catalysts with different Co and Ni loadings, respectively (λ = 0.24125 Å).

TEM and HRTEM studies were carried out to examine the morphology of the catalysts. **Figure 11a–d** displays TEM images for the fresh catalysts with the following metal loadings 3.3 wt% Co, 1.9 wt% Ni, 9.7 wt% Co, and 7.7 wt% Ni, respectively. While isolated Co_3O_4 and NiO nanoparticles can be identified for 3.3 wt% Co and 1.9 wt% Ni, respectively, in which both average particle size is about 10 nm in diameter (**figure 11a** and **11b**), segregated Co_3O_4 or NiO nanoparticles supported on ZnO could not be clearly distinguishable in the samples with higher metal loadings (**figure 11c** and **11d**). This is probably due to Co and Ni agglomeration and poor contrast between the support and Co_3O_4 or NiO nanoparticles. HRTEM images (**Figure 11e-h**) demonstrate that the catalysts display a high crystallinity, in which lattice fringes could be clearly observed. The ZnO phase almost exclusively exposes (002) crystallographic planes which corresponds to a lattice parameter of 2.6 Å (**figure 11e** and **11f**). [92,109] As shown in **figure**

11e and **11g**, continuous lattice fringes with an interplanar d-spacing of 2.9 Å and 2.3 Å matched well with the (220) and (222) planes of the Co_3O_4 phase, respectively, whereas lattice spacing of 2.1 Å could be assigned to the (200) planes of the NiO phase (**figure 11f** and **11h**).[92,109–111] HRTEM results also demonstrate that Co_3O_4 or NiO are in close contact with ZnO, indicating that a heterojunction between Co or Ni oxide phases and ZnO support was effectively obtained.

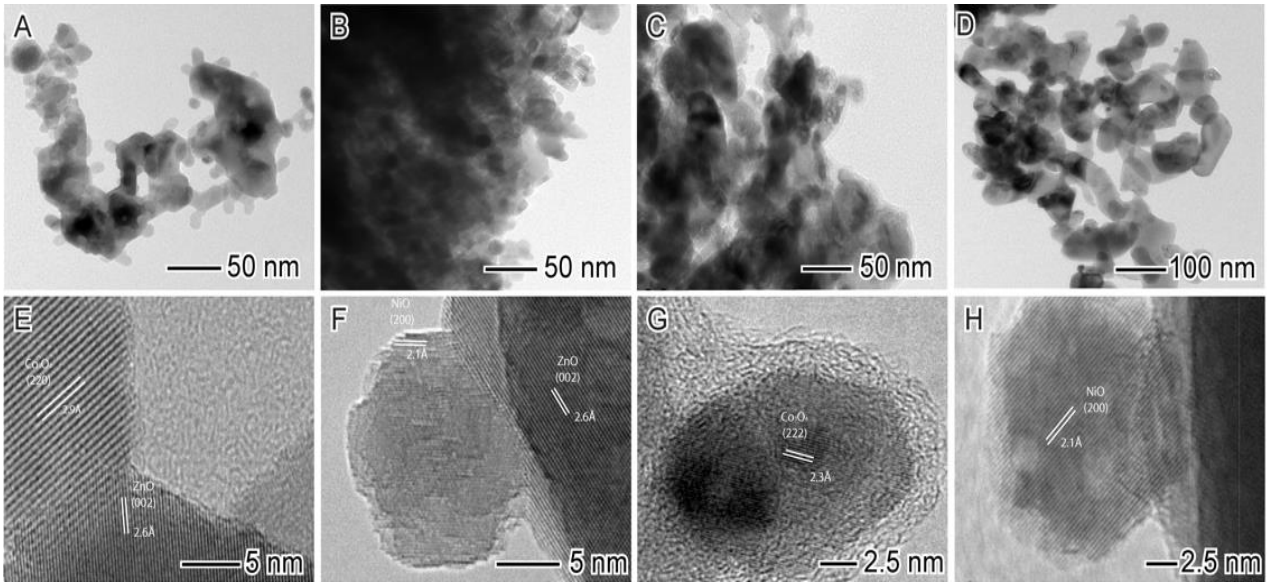

Figure 11. Representative TEM and HRTEM images of Co/ZnO and Ni/ZnO catalysts. (a) and (e): 3.3 wt% Co/ZnO; (b) and (f): 1.9 wt% Ni/ZnO, (c) and (g): 9.7 wt% Co/ZnO; (d) and (h): 7.7 wt% Ni/ZnO.

The catalytic performance for the CO_2 hydrogenation reaction over "x" wt% Co/ZnO catalysts, the ZnO support, and pure Co oxides as controls are summarized in **Figure 12**. As can be observed, the as-prepared catalysts were evaluated in the temperature range of 150 to 450 °C, under a relatively moderate space velocity of 75 000 mL/g_{cat}/h. **Figure 12a** shows that the CO_2 conversion increases with increasing Co loading up to 18.3 wt% at all tested temperatures. The 18.3 wt% Co/ZnO catalyst also exhibited higher CO_2 conversion (72% and 79% at 350 and 450°C, respectively) than both

of the pure Co-oxides and the ZnO support at temperatures of 350 and 450°C. In terms of selectivity, **figure 12b** and **12c** reveal that the CO_2 methanation process was favored over the reverse water gas shift (RWGS) reaction as the Co content increased. These results are in agreement with previous reports showing that Co generally acts as a poor RWGS catalysts since it cleaves the C−O bond and catalyzes Fischer−Tropsch chemistry.[114–116] The high selectivity towards CH_4 for pure Co_3O_4 suggests that this oxide phase (upon reduction) is responsible for the catalytic activity and selectivity behavior of Co/ZnO catalyst rather than that of pure Co_2O_3 phase, which display a poor selectivity towards CH_4. This observation is n agreement with the XRD findings in which nearly all Co/ZnO materials show characteristic diffraction peaks of Co_3O_4 phase. The catalytic activities of Co/ZnO catalysts for the CO_2 methanation were also investigated. It was found that 5.4 wt% Co and 16.3 wt% Co materials showed the highest activities at 350°C and 250 °C, respectively (**figure 12d**). It is noteworthy that only at 250°C all catalysts displayed CO_2 conversion below 5% (**figure 12a**). This implicates that only at this temperature their CO_2 conversion are in the kinetic region. Therefore, it is safer to consider the catalytic activity at 250°C as being more accurate.

The as-prepared Ni/ZnO catalysts were evaluated towards the same aforementioned CO_2 hydrogenation reaction conditions used for Co/ZnO catalyts (**Figure 13**). **Figure 13a** shows that the CO_2 conversion increased with increasing the wt% of Ni loading up to 7.7 wt%, followed by a decrease. **Figure 13b** and **13c** illustrate the impact of the amount of Ni loading on the selectivity behavior of such catalyts. All catalysts displayed an excellent performance for the RWGS reaction, exhibiting selectivity towards CO higher than 95% at all tested temperatures, even for the highest

Ni loading. This result is quite unexpected since many reports have shown that Ni is a high active and selective CO_2 methanation metal catalyst.[36,89,117,118]

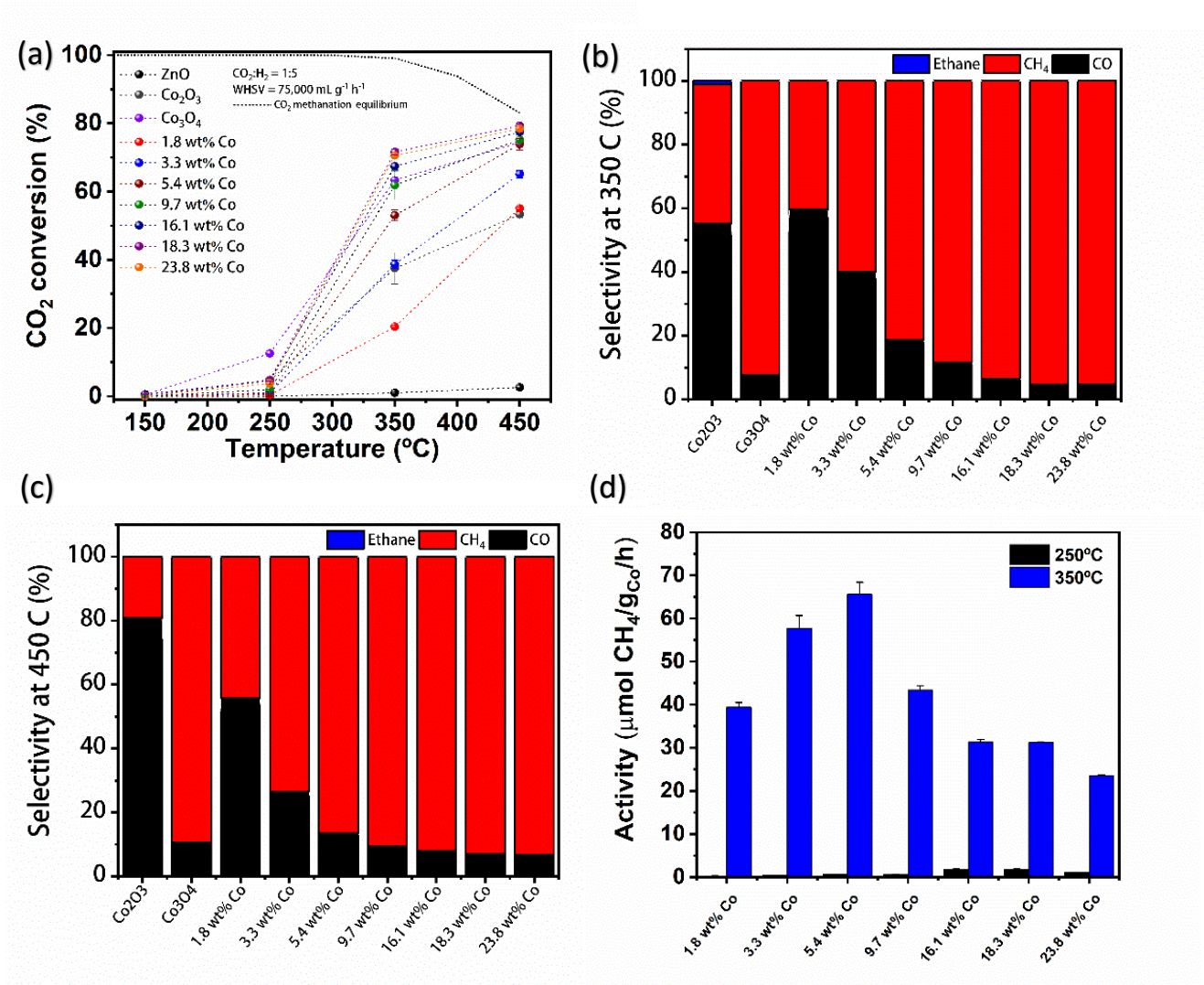

Figure 12. Catalytic performance for Co/ZnO catalysts as a function of the Co loading: (a) CO_2 conversion, (b) product selectivity at 350°C, (c) product selectivity at 450°C, (d) CH_4-generated rates.

Although there have been reports showing that Ni supported catalysts with high selectivity towards CO can be obtained by alloying Ni with other metals such as iron (Fe) or even by using Ni nanoparticles smaller than 2nm, these results cannot be properly compared to our catalyst system.[36,38,119] This is because our prepared NiO nanoparticles are about 10nm in diameter and, at least in principle, no alloying process on Ni was

utilized. The activity per unit nickel was observed to decrease with increasing Ni concentration (**figure 13d**). This may be due to eventual metal agglomeration at high Ni loadings leading to larger nanoparticle sizes and thus reduced exposure of catalytic sites available on the surface for the RWGS reaction.

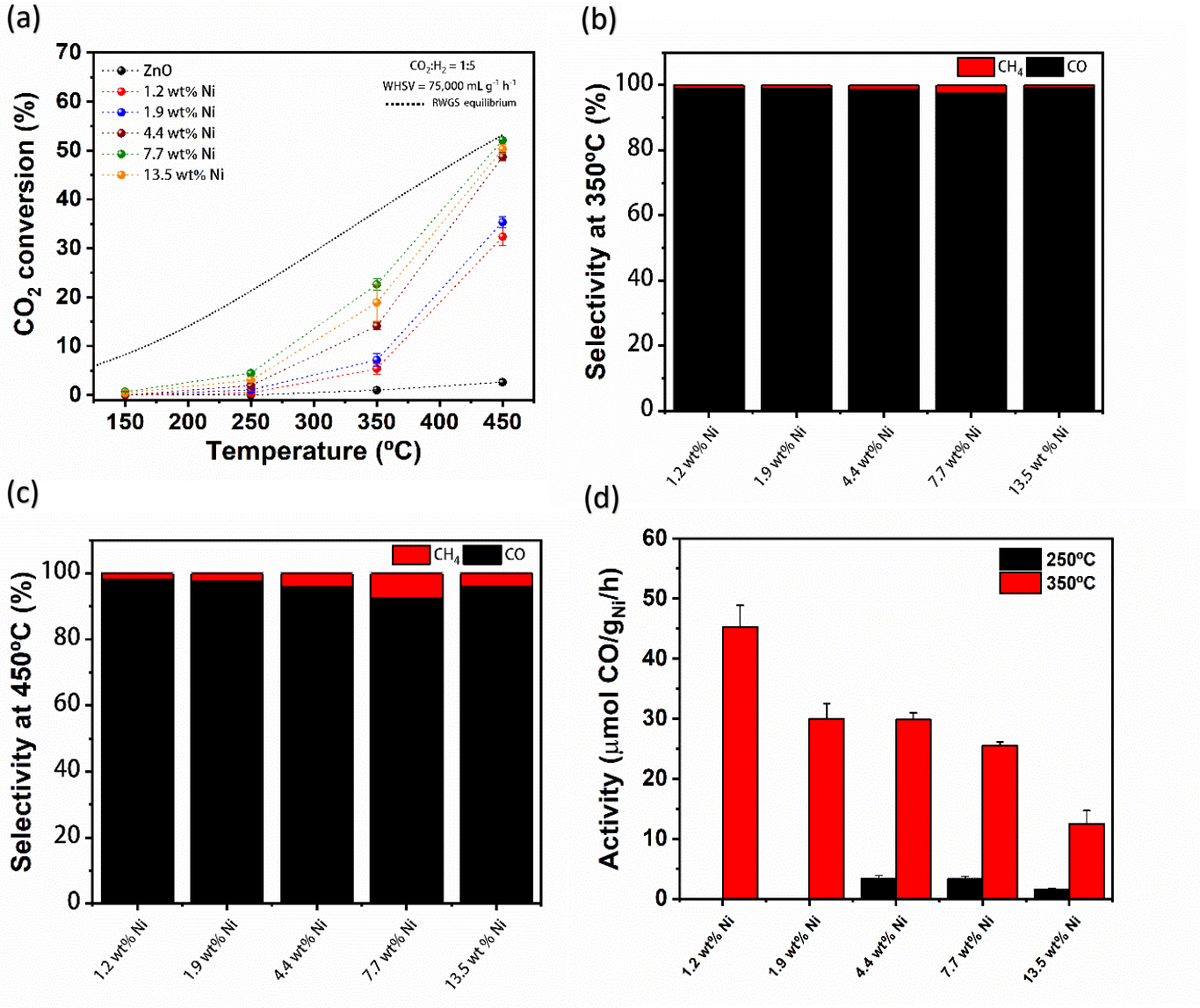

Figure 13. Catalytic performance for Ni/ZnO catalysts as a function of the Ni loading. (a) CO_2 conversion, (b) product selectivity at 350°C, (c) product selectivity at 450°C, (d) CO-generated rates of all tested catalysts.

To verify whether or not ZnO support plays a significant role on such selectivity behavior, we prepared catalysts with the same Ni loading supported on commercial

ZnO, titanium oxide (TiO_2), and cerium oxide (CeO_2). We then compared their selectivity relative to our catalyst. As shown in **figure 14a** and **14b**, Ni supported on ZnO displayed a high selectivity towards CO (98%), whereas Ni/TiO_2 or Ni/CeO_2 produced considerable amount of methane. These observations suggest that metal−support interactions between Ni and ZnO strongly affects the catalytic selectivity performance to produce more CO over CH_4. Regarding the stability of our catalyst system, we selected the 1.9wt% Ni sample as a representative catalyst and tested its stability at 450 °C. As shown in **figure 14c**, no significant loss of catalytic activity or selectivity after 20h under continuous RWGS reaction conditions.

In principle, studying heterogeneous catalytic processes at a molecular level is extremely challenging.[95,120] Catalyst surfaces can undergo chemical and structural transformations during reactions, which can radically alter their initial composition and impact catalytic performances.[48,95,120,121] Therefore, such study requires conducting investigations on the structural, electronic and surface chemistry properties of catalysts under reaction conditions.[95,120,121]

In this context, advances in surface science has provided a large number of *in situ* and *operando* experimental techniques that have proved to be powerful tools for carrying out these investigations on such conditions.[121–124] Among those, ambient pressure X-ray photoelectron spectroscopy (AP-XPS) is certainly one of the most versatile *in situ* methods.[125–127] In particular, it can provide quantitative information on the elemental composition and chemical specificity (e.g. oxidation state) of catalyst surfaces on the atomic scale.[126,128] In addition, its ability to unravel reaction chemistry and catalyst active phases has been demonstrated (even at pressures of up to 130 mbar, which are typically undetectable by high vacuum XPS or other ex situ studies).[95,126,127]

Finally, AP-XPS enables the correlation of reaction kinetics/mechanisms to surface composition and chemical/electronic states under catalytically relevant pressure, temperature, and atmosphere conditions. [120,123,126,127,129,130]

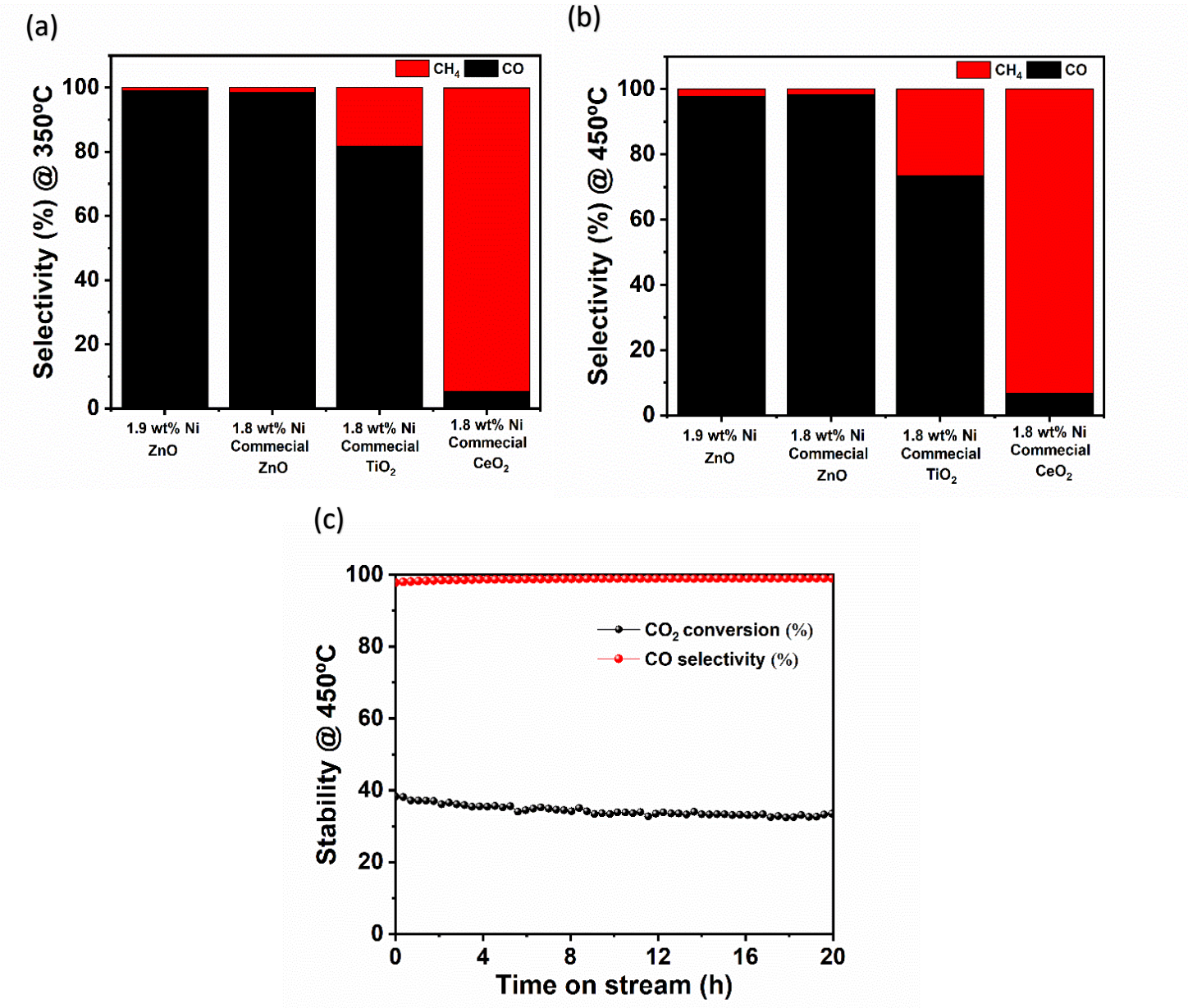

Figure 14. Catalytic selectivity at 350°C (a) and 450°C (b) for the 1.9 wt% Ni sample and other catalysts with similar Ni loading supported on commercial ZnO, TiO_2, and CeO_2. (c) Stability test for the 1.9 wt% Ni sample showing both CO_2 conversion and product selectivity at 450°C as a function of time.

Given the outstanding capabilities of such *in situ* technique, AP-XPS experiments were conducted for the 1.9wt% Ni/ZnO, 7.7%wt Ni/ZnO, 3.3%wt Co/ZnO, and 9.7%wt Co/ZnO samples to probe such catalytic surfaces and provide further information regarding the surface oxidation state of the catalysts at the gas−solid interface under reaction conditions such as elevated temperature and moderate background pressure of CO_2/H_2. **Figures 15a-f** summarize all Co 2p XPS and Zn LMM Auger electron spectra for the selected Co/ZnO catalysts acquired after exposing them to reaction conditions. As shown in figure **15a** and **15b**, the Co 2p XPS region for both 3.3 wt% Co/ZnO, and 9.7 wt% Co/ZnO samples revealed that Co_3O_4 is reduced to metallic Co after H_2 pretreatment (20mbar) at 400 °C.[112,131] It is also observed that, when exposed to both reactant gases (5 mTorr of CO_2, and 25 mTorr of H_2) at room temperature or higher temperatures (250, 350, and 450°C), cobalt still retained its metallic form. Contrary to Co_3O_4, the Zn LMM Auger electron spectra for both tested catalysts (**figure 15d** and **15e**) demonstrate that ZnO support does not undergo any significant reduction process.[83,131] These observations suggest that Co^0 (ca. 778.1 or 778.3 eV) was the active state responsible for the CO_2 hydrogenation conversion in the two Co/ZnO catalysts. By changing the gas atmosphere conditions to CO_2 only (30mbar), the reoxidation of metallic Co to CoO oxide at temperatures higher than 250°C (**figure 15c**) was detected.[131,132] This CoO oxide phase was also observed in HRTEM images of such catalyst taken after reaction (**figure 17a**). As expected, **figure 15f** shows that ZnO support did not oxidize or reduce under CO_2 atmosphere only. These results suggest that metallic Co acts as the active site to activate CO_2. It is also clear that Co^0 does not show any signal of reoxidation when both reactant gases (CO_2 and H_2) are added to the

reaction (**figure 15a** and **15b**) due to the high content of H_2 available that can rapidly reduce any formed CoO oxide back to Co^0.

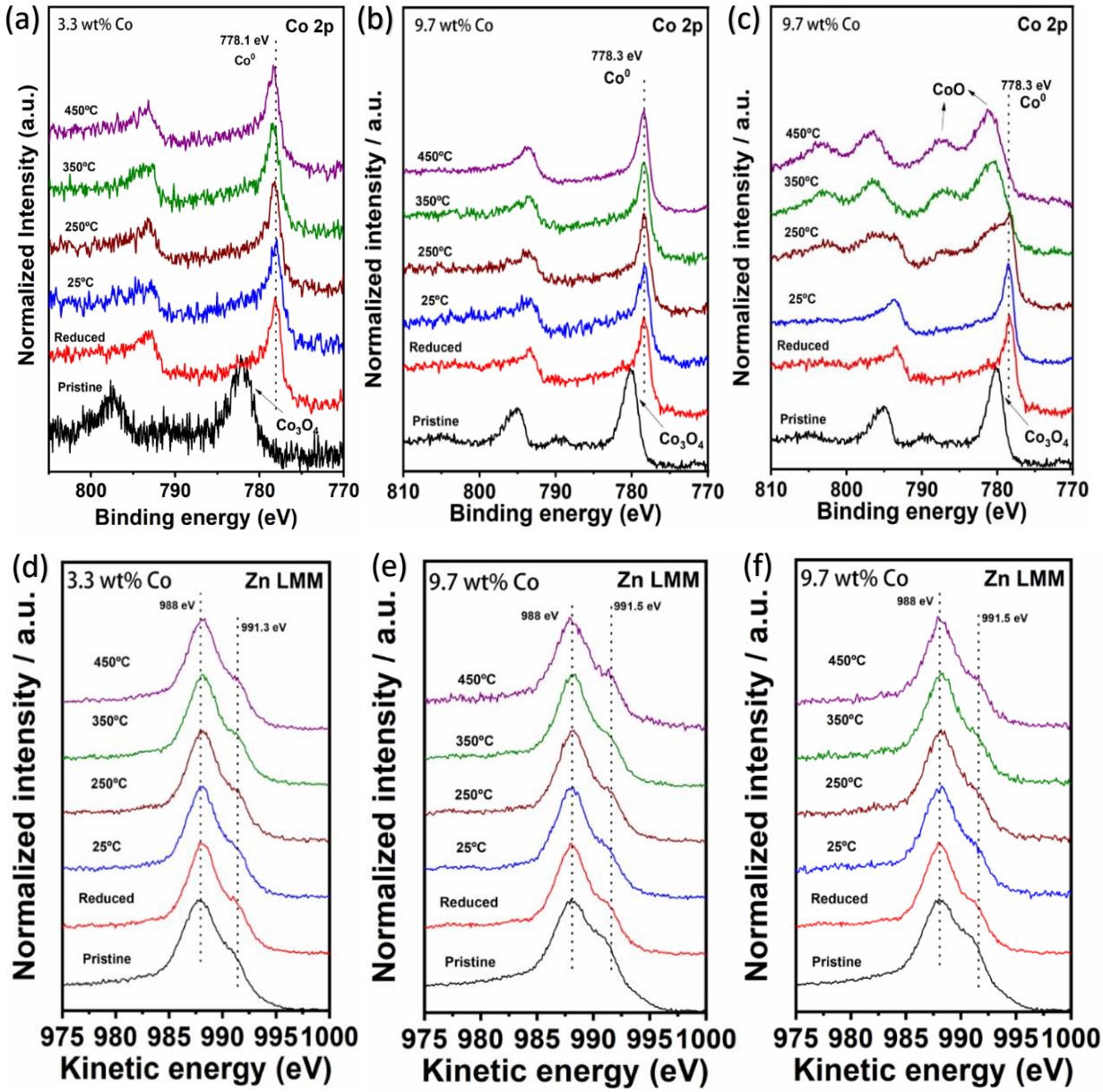

Figure 15. AP-XPS profiles in the Co 2p, and Zn LMM Auger regions of selected Co/ZnO catalyts. AP-XPS profiles displayed in (a), (b), (d), and (e) were collected under CO_2 hydrogenation reaction conditions (5 mTorr of CO_2 + 25 mTorr of H_4). AP-XPS Profiles shown in (c) and (f) were collected under CO_2 atmosphere only (30 mTorr of CO_2). All measurements were performed as the following order: 1.(Pristine) as-prepared catalyst at 25 °C, 2. (Reduced) cooled to 25 °C after 0.5 h of H_2 pretreatment at 400 °C, and 3. during the CO_2 hydrogenation reaction at 25, 250, 350, and 450 °C, respectively.

Ambient pressure Ni 2p and Zn LMM XPS measurements were conducted on the 1.9 wt% Ni/ZnO and 7.7 wt% Ni/ZnO samples in the presence of 5 mTorr of CO_2 and 25 mTorr of H_2 to simulate reverse water-gas shift reaction conditions (**Figure 16a-f**). In **figure 16a** and **16b**, we display the Ni 2p region for both Ni-based catalyts. Like what is observed for cobalt containing catalyts, one can see that NiO oxide is reduced to metallic Ni after H_2 pretreatment (20mbar) at 400 °C. Upon exposure to reactant gases, Ni catalysts also retain its Ni^0 state even at elevated temperatures (450°C). However, the binding energy (BE) of Ni^0 (852.9eV) for both catalyts is shifted towards higher BE by 0.3eV relative to the Ni^0 foil (852.6 eV).[123,131] This shift has also been reported for some Ni/TiO_2 surfaces.[123] They also found that such shifting in BE correlates well with CO binding less strongly to such Ni^0 surfaces.[123] Contrary to that Zhang and co-workers[117] using *in situ* XPS experiments have reported, no such shifting in BE was detected for Ni^0 for a high active and selective CO_2 methanation Ni/CeO_2 catalyst. These observations suggest that once CO is formed, it is unlikely to strongly adsorb on the Ni^0 surface of our catalysts. Some of the most likely CO_2 hydrogenation mechanisms indicate that CO_2 is first hydrogenated to CO, which is then further reduced to CH_4.[36,91,133] In this context, CO is not expected to be further hydrogenated to CH_4 for our catalytic system which could explain the found high CO selectivity. **Figure 16d** and **16e** display the Zn LMM Auger spectra for the tested samples. As can be observed, the 7.7wt% Ni/ZnO sample show clearly a peak at 992eV that increases as temperature increases. This peak can be assigned to the presence of Zn^0 which indicates that ZnO support was reduced to some extent.[83,131] As shown in **figure 16c** and **16h**, when CO_2 was the only (30mbar) reactant gas in the chamber, a slight amount of metallic Ni but all formed Zn^0 are reoxidized to

NiO and ZnO, respectively. It is worth to mention that HRTEM images of such catalyst reveal that both Ni and NiO phases are present in the catalyst surface (**figure 17b).** These results suggest that either bimetallic Ni-Zn alloys or segregated Ni and Zn metallic phases are formed in our catalyst during reaction conditions and are probably responsible for the CO_2 activation and conversion to CO.

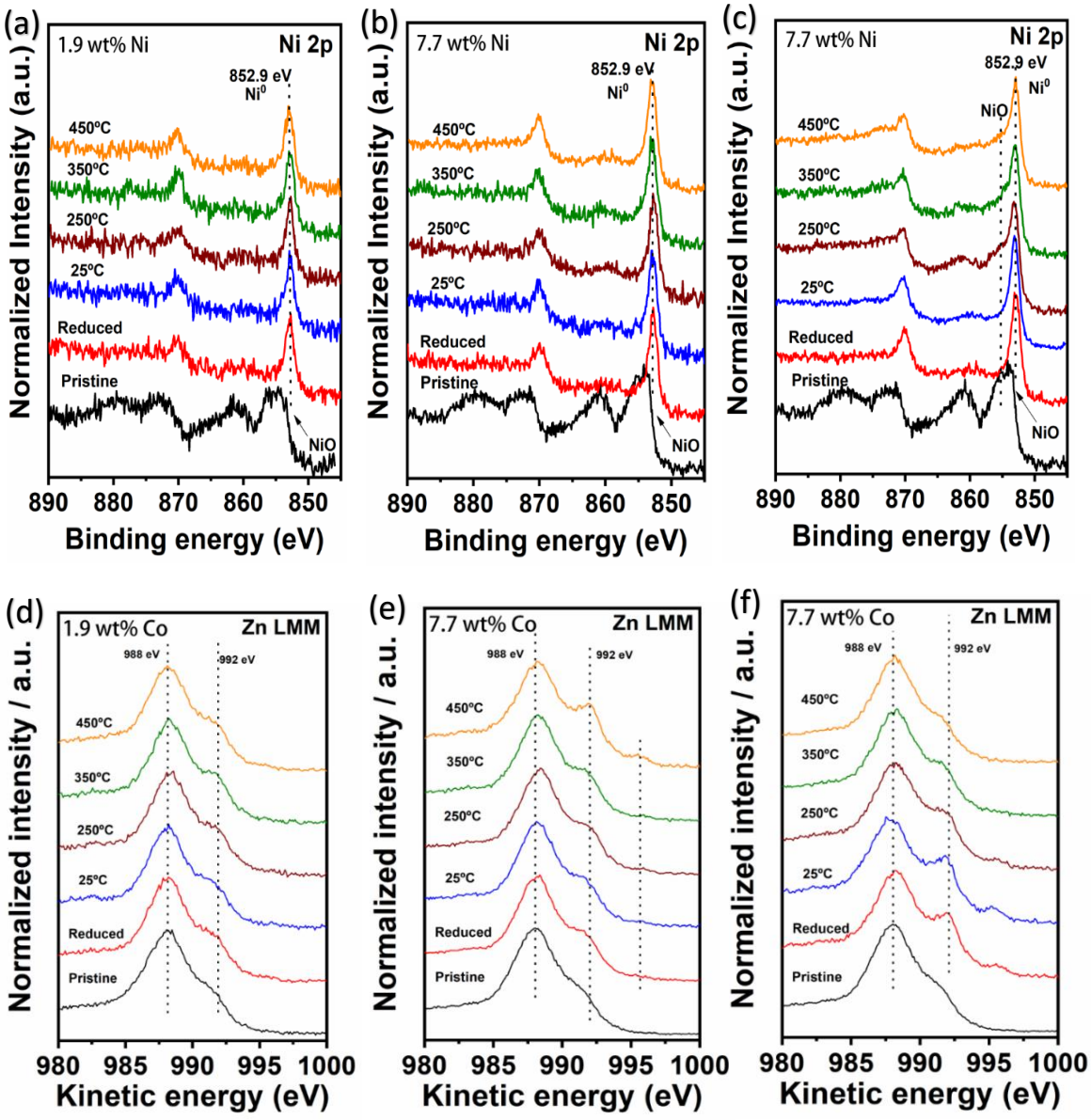

Figure 16. AP-XPS profiles in the Co 2p, and Zn LMM Auger regions of selected Ni/ZnO catalyts. AP-XPS profiles displayed in (a), (b), (d), and (e) were collected under CO_2 hydrogenation reaction conditions (5 mTorr of CO_2 + 25 mTorr of H_2). AP-XPS Profiles shown in (c) and (f) were collected under CO_2 atmosphere only (30 mTorr of CO_2). All measurements were performed as the following order: 1.(Pristine) as-prepared catalyst

at 25 °C, 2. (Reduced) cooled to 25 °C after 0.5 h of H_2 pretreatment at 400 °C, and 3. during the CO_2 hydrogenation reaction at 25, 250, 350, and 450 °C, respectively.

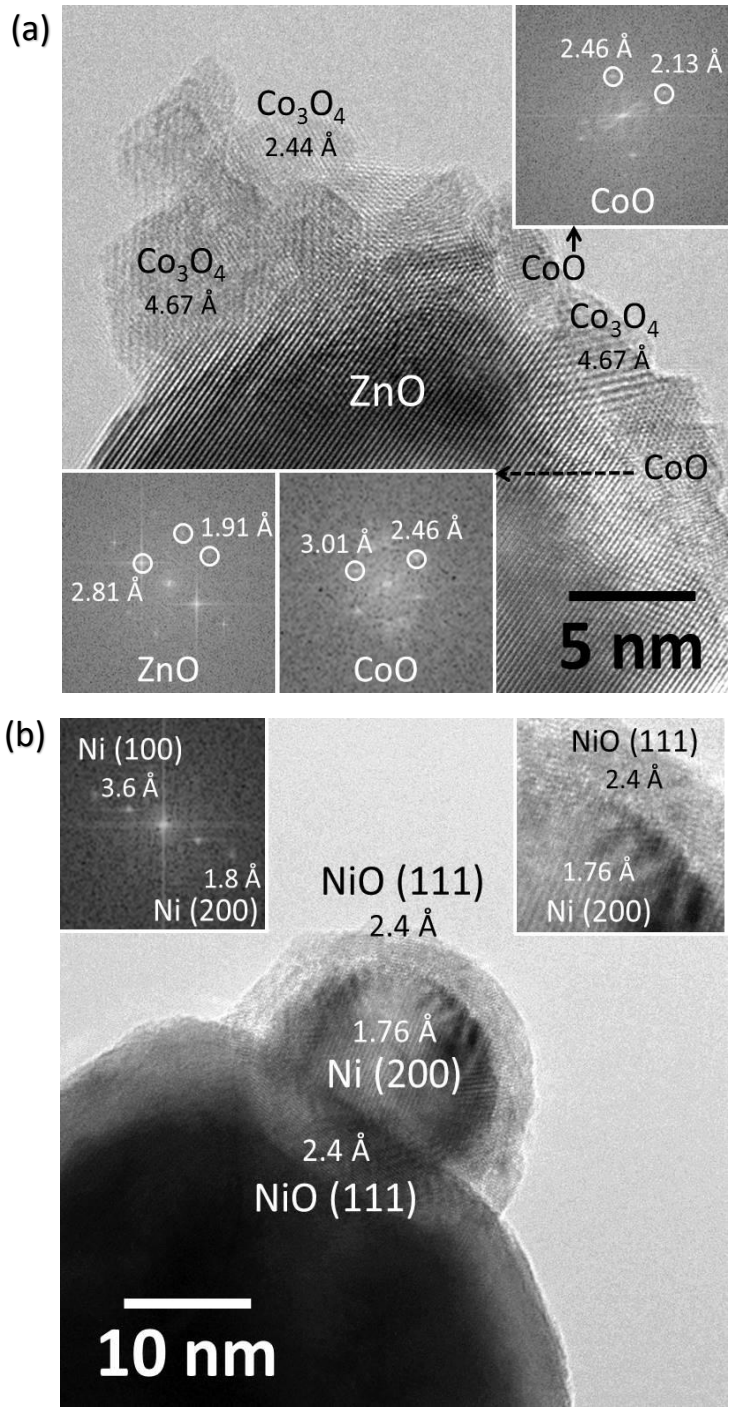

Figure 17. Representative HRTEM images of post-reaction 9.4 wt% Co/ZnO (a) and 7.7 wt% Ni/ZnO (b) catalysts.

In order to further rationalize the structural behavior of Ni/ZnO catalysts, we investigated these materials using time-resolved X-ray diffraction (XRD). This *in situ* technique is another equally important powerful tool for studying the behavior of heterogeneous catalysts under reaction conditions. Particularly, it offers a way to identify the active phase of such catalyst materials and to account for crystal structure changes that can take place upon interaction of those with the reactants and products. [134,135]

As illustrated in **Figure 18a**, the as-prepared 1.9 wt% Ni/ZnO catalyst is composed of NiO species dispersed on ZnO. Additionally, one can see that when exposing the sample to a hydrogen reduction process by gradually heating it from room temperature to 400 °C under H_2 atmosphere, neither the nickel oxide (2θ = 6.56º) nor ZnO phase were fully reduced to metallic Ni and Zn, respectively. In fact, no significant signal for such metallic phases could be identified. On the other hand, the diffraction patterns revealed a freshly formed phase (2θ = 7.58°) starting at ∼220 °C. This can be assigned to the presence of a NiZn alloy phase. [136,137] Upon exposure to reactant gases (**figure 18b**), this NiZn alloy phase remained stable and no dealloying process was observed from room temperature up to 450 °C. Also, the evolution of additional phases was not verified during the reaction. These results suggest that CO_2 in the reactant stream, when combined with H_2, is not capable of oxidizing the NiZn alloy phase. More importantly, these results corroborate with those of AP-XPS and suggest that bimetallic NiZn alloy may work as the active phase for the hydrogenation of CO_2 to CO. Moreover, it may be also responsible for the selective behavior displayed by such catalyts. In particular, as it has been recently showed by Cheng and coworkers[36] that alloying Ni with another metal (e.g. Fe) resulted in a catalyst system with high selectivity towards CO.

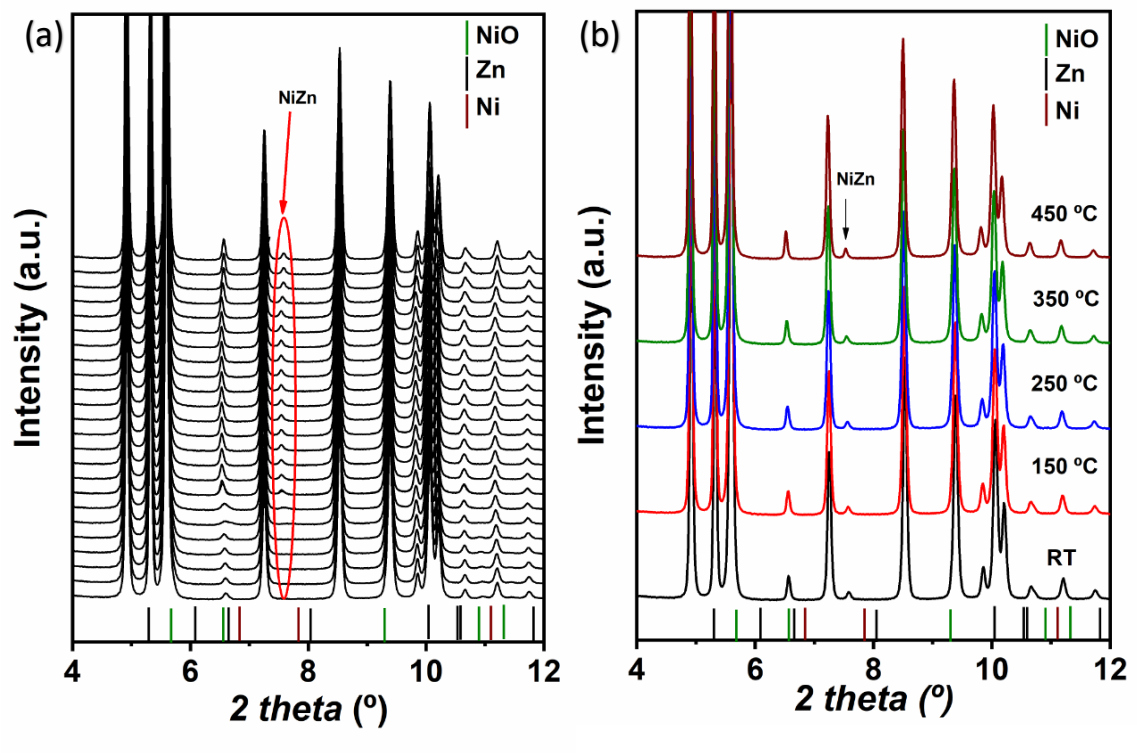

Figure 18. In situ time-resolved XRD patterns for 1.9 wt% Ni/ZnO catalyst during H_2 pretreatment (6mL/min H_2) up to 400°C (a), and (b) prereduced under RWGS reaction conditions at different temperatures (2ml/min CO_2 : 6 ml/min H_2).

5. CONCLUSIONS

In this thesis we have developed and investigated catalyst systems based on earth abundant 3d metals that hold outstanding potential for applications in energy conversion processes. In this case, we focused on the oxygen evolution reaction (OER) and the hydrogenation of CO_2 to fuels and value-added chemicals.

Regarding the OER studies, we developed a solvothermal synthetic method in which mixed Ni-Fe oxyhydroxides were formed and mixed with a carbon structure, resulting in hybrid organic-inorganic material. This system displayed an outstanding OER catalytic performance. We believe that the proposed synthetic method represents a promising way to generate hybrid Ni-Fe-based electrocatalysts with highly catalytic activity for OER. The remarkable enhancement of the OER performance may be ascribed to several factors. For instance, it included the synergistic electronic interplay of Ni and Fe in Ni-Fe$(OH)_2$ during the oxidation reaction. Also, in the case of $Ni_{75}Fe_{25}(OH)_2$, the presence of mixed valence Fe^{2+}/Fe^{3+} ions may play a significant role on its intrinsic superior OER catalytic activity. Another important factor was the incorporation of carbon to the oxyhydroxide structures. In this case, carbon may benefit the final composite electrocatalyst materials as it can help to enhance their conductivity and expose more surface catalytic active sites for the OER. Despite these promising results, more detailed studies on the effects of high surface-area conductive supports and metal content still need to be addressed. In this way, we believe that new insights may contribute to draw more complete conclusions about the high OER performance of our catalysts s. This, in turn, can also offer a way to advance in the design of new high-performing OER electrocatalysts.

Regarding the CO_2 hydrogenation reaction, we developed two catalysts: Co/ZnO and Ni/ZnO displaying by varying Co or Ni loadings on a ZnO support. The resulting Ni/ZnO and Co/ZnO materials exhibited high catalytic activity for the RWGS or CO_2 methanation reactions, respectively. Additionally, these Ni and Co-based catalysts displayed an outstanding selectivity performance, in which both CO or CH_4 reaction products could be obtained with selectivity higher than 95%. These remarkable catalytic activity and selectivity behavior may be ascribed to several factors. Ex situ XRD results revealed that Co_3O_4 and NiO are the corresponding crystalline phase obtained after calcination of the as-prepared Co/ZnO and Ni/ZnO catalysts, respectively. By examining the reaction of CO_2 hydrogenation with Co/ZnO and Ni/ZnO using ambient-pressure X-ray photoelectron spectroscopy (AP-XPS) studies, it was found that both Co_3O_4 and NiO phases have their surfaces fully reduced to metallic Co and Ni, respectively, under the tested CO_2 hydrogenation reaction conditions. These observations suggest that such metallic phases, when associated with the ZnO support, correspond the catalytic active phases in the reaction. *In situ* time resolved X-ray Diffraction (*in situ* TR-XRD) experiments further enlighten our understanding of the Ni/ZnO catalysts. These studies demonstrated that a NiZn alloy phase is formed during reaction, which may be ascribed as the possible active phase responsible for both the catalytic activity and selectivity of the Ni/ZnO catalyst. Overall, we were able to correlate the catalytic performance and dynamic evolution in the chemical composition of our catalyst systems under reaction conditions. This has provided us with means to demonstrate the importance of metal−oxide interactions for the activation of CO_2 on Co/ZnO NS Ni/ZnO catalysts. However, even with these very promising results, more detailed studies still need to be done. In this context, we are currently studying these systems using Brunauer-Emmett-

Teller (BET) surface area analysis (BET), temperature-programmed reduction analysis (TPR), and operando X-ray absorption fine structure analysis (XAFS).

We believe that the results provided by these new studies will shed new knowledge into the effects of metal-support interactions in the reported catalytic systems, contributing to a better understanding over their catalytic behavior and performances in terms of activity and selectivity. Overall, we believe the results described herein already shed important insights into building the type of fundamental understanding that can enable us, in more rational and efficient terms, to design and optimize highly active and selective heterogeneous catalysts for the aforementioned energy conversion processes.

6. REFERENCES

1. Zhang, W., Lai, W. & Cao, R. Energy-Related Small Molecule Activation Reactions: Oxygen Reduction and Hydrogen and Oxygen Evolution Reactions Catalyzed by Porphyrin- and Corrole-Based Systems. *Chem. Rev.* **117,** 3717–3797 (2017).
2. Artz, J. *et al.* Sustainable Conversion of Carbon Dioxide: An Integrated Review of Catalysis and Life Cycle Assessment. *Chem. Rev.* **118,** 434–504 (2018).
3. Karl, T. R. Modern Global Climate Change. *Science (80-.).* **302,** 1719–1723 (2003).
4. Olah, G. A., Prakash, G. K. S. & Goeppert, A. Anthropogenic chemical carbon cycle for a sustainable future. *J. Am. Chem. Soc.* **133,** 12881–12898 (2011).
5. Mac Dowell, N., Fennell, P. S., Shah, N. & Maitland, G. C. The role of CO2 capture and utilization in mitigating climate change. *Nat. Clim. Chang.* **7,** 243–249 (2017).
6. Xu, S. & Carter, E. A. Theoretical Insights into Heterogeneous (Photo)electrochemical CO 2 Reduction. *Chem. Rev.* acs.chemrev.8b00481 (2018). doi:10.1021/acs.chemrev.8b00481
7. Álvarez, A. *et al.* Challenges in the Greener Production of Formates/Formic Acid, Methanol, and DME by Heterogeneously Catalyzed CO2Hydrogenation Processes. *Chem. Rev.* **117,** 9804–9838 (2017).
8. Sordakis, K. *et al.* Homogeneous Catalysis for Sustainable Hydrogen Storage in Formic Acid and Alcohols. *Chem. Rev.* **118,** 372–433 (2018).
9. Jin, H. *et al.* Emerging Two-Dimensional Nanomaterials for Electrocatalysis. *Chem. Rev.* **118,** 6337–6408 (2018).

10. Zhang, Q., Uchaker, E., Candelaria, S. L. & Cao, G. Nanomaterials for energy conversion and storage. *Chem. Soc. Rev.* **42,** 3127–3171 (2013).

11. Wang, W. H., Himeda, Y., Muckerman, J. T., Manbeck, G. F. & Fujita, E. CO2 Hydrogenation to Formate and Methanol as an Alternative to Photo- and Electrochemical CO2 Reduction. *Chem. Rev.* **115,** 12936–12973 (2015).

12. Sordakis, K. *et al.* Homogeneous Catalysis for Sustainable Hydrogen Storage in Formic Acid and Alcohols. *Chem. Rev.* acs.chemrev.7b00182 (2017). doi:10.1021/acs.chemrev.7b00182

13. Goeppert, A., Czaun, M., Jones, J.-P., Surya Prakash, G. K. & Olah, G. A. Recycling of carbon dioxide to methanol and derived products – closing the loop. *Chem. Soc. Rev.* **43,** 7995–8048 (2014).

14. Staffell, I. *et al.* The role and status of hydrogen and fuel cells across the global energy system. *engrXiv* (2018). doi:10.17605/OSF.IO/RZM4G

15. Zou, X. & Zhang, Y. Noble metal-free hydrogen evolution catalysts for water splitting. *Chem. Soc. Rev.* **44,** 5148–5180 (2015).

16. Dodds, P. E. *et al.* Hydrogen and fuel cell technologies for heating: A review. *Int. J. Hydrogen Energy* **40,** 2065–2083 (2015).

17. Song, F. *et al.* Transition Metal Oxides as Electrocatalysts for the Oxygen Evolution Reaction in Alkaline Solutions: An Application-Inspired Renaissance. *J. Am. Chem. Soc.* **140,** 7748–7759 (2018).

18. Turner, J. A. A Realizable Renewable Energy Future. *Science (80-.).* **285,** 687–689 (1999).

19. Tollefson, J. Hydrogen vehicles: Fuel of the future? *Nature* **464,** 1262–1264 (2010).

20. Roger, I., Shipman, M. A. & Symes, M. D. Earth-abundant catalysts for electrochemical and photoelectrochemical water splitting. *Nat. Rev. Chem.* **1,** 0003 (2017).

21. Hunter, B. M., Gray, H. B. & Müller, A. M. Earth-Abundant Heterogeneous Water Oxidation Catalysts. *Chem. Rev.* **116,** 14120–14136 (2016).

22. Trotochaud, L., Young, S. L., Ranney, J. K. & Boettcher, S. W. Nickel − Iron Oxyhydroxide Oxygen-Evolution Electrocatalysts : The Role of Intentional and Incidental Iron Incorporation. (2014). doi:10.1021/ja502379c

23. Jiang, J. *et al.* Atomic-level insight into super-efficient electrocatalytic oxygen evolution on iron and vanadium co-doped nickel (oxy)hydroxide. *Nat. Commun.* 1–12 (2018). doi:10.1038/s41467-018-05341-y

24. Go, M. *et al.* Tracking Catalyst Redox States and Reaction Dynamics in Ni − Fe Oxyhydroxide Oxygen Evolution Reaction Electrocatalysts : The Role of Catalyst Support and Electrolyte pH. (2017). doi:10.1021/jacs.6b12250

25. Montoya, J. H. *et al.* Materials for solar fuels and chemicals. *Nat. Mater.* **16,** 70–81 (2016).

26. Linic, S., Christopher, P. & Ingram, D. B. Plasmonic-metal nanostructures for efficient conversion of solar to chemical energy. *Nat. Mater.* **10,** 911–921 (2011).

27. Aslam, U., Rao, V. G., Chavez, S. & Linic, S. Catalytic conversion of solar to chemical energy on plasmonic metal nanostructures. *Nat. Catal.* **1,** 656–665 (2018).

28. Stamenkovic, V. R., Strmcnik, D., Lopes, P. P. & Markovic, N. M. Energy and fuels from electrochemical interfaces. *Nat. Mater.* **16,** 57–69 (2016).

29. Zhou, Q. *et al.* Active-Site-Enriched Iron-Doped Nickel/Cobalt Hydroxide Nanosheets for Enhanced Oxygen Evolution Reaction. *ACS Catal.* **8,** 5382–5390 (2018).

30. Rodriguez, J. A. *et al.* Hydrogenation of CO2 to Methanol: Importance of Metal-Oxide and Metal-Carbide Interfaces in the Activation of CO2. *ACS Catal.* **5,** 6696–6706 (2015).

31. Jia, J. *et al.* Heterogeneous catalytic hydrogenation of CO_2 by metal oxides: defect engineering – perfecting imperfection. *Chem. Soc. Rev.* **46,** 4631–4644 (2017).

32. Fan, L.-S., Zeng, L., Wang, W. & Luo, S. Chemical looping processes for CO2 capture and carbonaceous fuel conversion – prospect and opportunity. *Energy Environ. Sci.* **5,** 7254 (2012).

33. Aresta, M., Dibenedetto, A. & Angelini, A. Catalysis for the valorization of exhaust carbon: From CO2 to chemicals, materials, and fuels. technological use of CO2. *Chem. Rev.* **114,** 1709–1742 (2014).

34. Ghoussoub, M., Xia, M., Duchesne, P. N., Segal, D. & Ozin, G. Principles of photothermal gas-phase heterogeneous CO_2 catalysis. *Energy Environ. Sci.* (2019). doi:10.1039/C8EE02790K

35. Rodriguez, J. A. *et al.* Hydrogenation of CO2to Methanol: Importance of Metal-Oxide and Metal-Carbide Interfaces in the Activation of CO2. *ACS Catal.* **5,** 6696–6706 (2015).

36. Winter, L. R., Gomez, E., Yan, B., Yao, S. & Chen, J. G. Tuning Ni-catalyzed CO2hydrogenation selectivity via Ni-ceria support interactions and Ni-Fe bimetallic formation. *Appl. Catal. B Environ.* **224,** 442–450 (2018).

37. Porosoff, M. D., Yu, W. & Chen, J. G. Challenges and opportunities in correlating bimetallic model surfaces and supported catalysts. *J. Catal.* **308,** 2–10 (2013).

38. Gonçalves, R. V. *et al.* Selective hydrogenation of CO2into CO on a highly dispersed nickel catalyst obtained by magnetron sputtering deposition: A step towards liquid fuels. *Appl. Catal. B Environ.* **209,** 240–246 (2017).

39. Rodriguez, J. A. *et al.* CO2hydrogenation on Au/TiC, Cu/TiC, and Ni/TiC catalysts: Production of CO, methanol, and methane. *J. Catal.* **307,** 162–169 (2013).

40. Schwach, P., Pan, X. & Bao, X. Direct Conversion of Methane to Value-Added Chemicals over Heterogeneous Catalysts: Challenges and Prospects. *Chem. Rev.* **117,** 8497–8520 (2017).

41. Dry, M. E. The Fischer-Tropsch process: 1950-2000. *Catal. Today* **71,** 227–241 (2002).

42. Schulz, H. Short history and present trends of Fischer-Tropsch synthesis. *Appl. Catal. A Gen.* **186,** 3–12 (1999).

43. Marques Mota, F. & Kim, D. H. From CO_2 methanation to ambitious long-chain hydrocarbons: alternative fuels paving the path to sustainability. *Chem. Soc. Rev.* **48,** 205–259 (2018).

44. Wang, W., Wang, S., Ma, X. & Gong, J. Recent advances in catalytic hydrogenation of carbon dioxide. *Chem. Soc. Rev.* **40,** 3703 (2011).

45. Burdyny, T. & Smith, W. A. CO_2 reduction on gas-diffusion electrodes and why catalytic performance must be assessed at commercially-relevant conditions. *Energy Environ. Sci.* (2019). doi:10.1039/C8EE03134G

46. Vogiatzis, K. D. *et al.* Computational Approach to Molecular Catalysis by 3d Transition Metals: Challenges and Opportunities. *Chem. Rev.* (2018).

doi:10.1021/acs.chemrev.8b00361

47. Lewis, N. S. A prospective on energy and environmental science. *Energy Environ. Sci.* (2019). doi:10.1039/C8EE90070A

48. Roduner, E. Understanding catalysis. *Chem. Soc. Rev.* **43,** 8226–8239 (2014).

49. Wang, D. & Astruc, D. The recent development of efficient Earth-abundant transition-metal nanocatalysts. *Chem. Soc. Rev.* **46,** 816–854 (2017).

50. Suen, N. T. *et al.* Electrocatalysis for the oxygen evolution reaction: Recent development and future perspectives. *Chem. Soc. Rev.* **46,** 337–365 (2017).

51. Dionigi, F. & Strasser, P. NiFe-Based (Oxy)hydroxide Catalysts for Oxygen Evolution Reaction in Non-Acidic Electrolytes. *Adv. Energy Mater.* **6,** (2016).

52. Liardet, L. & Hu, X. Amorphous Cobalt Vanadium Oxide as a Highly Active Electrocatalyst for Oxygen Evolution. *ACS Catal.* **8,** 644–650 (2018).

53. Jung, J. Il, Jeong, H. Y., Lee, J. S., Kim, M. G. & Cho, J. A bifunctional perovskite catalyst for oxygen reduction and evolution. *Angew. Chemie - Int. Ed.* **53,** 4582–4586 (2014).

54. Suntivich, J., May, K. J., Gasteiger, H. a, Goodenough, J. B. & Shao-horn, Y. A Perovskite Oxide Optimized for Molecular Orbital Principles - Supporting Online Material. *Science (80-.).* **334,** 2010–2012 (2011).

55. Dong, H. *et al.* Excellent oxygen evolution reaction of NiO with a layered nanosphere structure as the cathode of lithium-oxygen batteries. *RSC Adv.* **8,** 3357–3363 (2018).

56. Kuznetsov, D. A. *et al.* Tuning Redox Transitions via Inductive Effect in Metal Oxides and Complexes, and Implications in Oxygen Electrocatalysis. *Joule* **2,** 225–244 (2018).

57. Feng, L. L. *et al.* High-Index Faceted Ni3S2 Nanosheet Arrays as Highly Active and Ultrastable Electrocatalysts for Water Splitting. *J. Am. Chem. Soc.* **137,** 14023–14026 (2015).

58. Zhao, X. *et al.* Carbon dots decorated hierarchical NiCo2S4/Ni3S2 composite for efficient water splitting. *ACS Sustain. Chem. Eng.* **7,** acssuschemeng.8b05611 (2018).

59. Cai, Z. *et al.* Oxygen Evolution Reaction Hot Paper Introducing Fe 2 + into Nickel – Iron Layered Double Hydroxide : Local Structure Modulated Water Oxidation Activity. 9392–9396 (2018). doi:10.1002/anie.201804881

60. Corrigan, D. A. The Catalysis of the Oxygen Evolution Reaction by Iron Impurities in Thin Film Nickel Oxide Electrodes. *J. Electrochem. Soc.* **134,** 377 (1987).

61. Trotochaud, L., Young, S. L., Ranney, J. K. & Boettcher, S. W. Nickel-Iron oxyhydroxide oxygen-evolution electrocatalysts: The role of intentional and incidental iron incorporation. *J. Am. Chem. Soc.* **136,** 6744–6753 (2014).

62. Klaus, S., Cai, Y., Louie, M. W., Trotochaud, L. & Bell, A. T. Effects of Fe electrolyte impurities on Ni(OH)2/NiOOH structure and oxygen evolution activity. *J. Phys. Chem. C* **119,** 7243–7254 (2015).

63. Go, M. *et al.* Oxygen Evolution Reaction Dynamics , Faradaic Charge E ffi ciency , and the Active Metal Redox States of Ni − Fe Oxide Water Splitting Electrocatalysts. (2016). doi:10.1021/jacs.6b00332

64. Yin, S., Tu, W., Sheng, Y., Du, Y. & Kraft, M. A Highly Efficient Oxygen Evolution Catalyst Consisting of Interconnected Nickel – Iron-Layered Double Hydroxide and Carbon Nanodomains. **1705106,** 1–9 (2018).

65. Chia, X. & Pumera, M. Characteristics and performance of two-dimensional

materials for electrocatalysis. *Nat. Catal.* **1,** 909–921 (2018).

66. Liu, M. H., Chen, Y. W., Lin, T. S. & Mou, C. Y. Defective Mesocrystal ZnO-Supported Gold Catalysts: Facilitating CO Oxidation via Vacancy Defects in ZnO. *ACS Catal.* **8,** 6862–6869 (2018).

67. Wang, Y. & Wöll, C. IR spectroscopic investigations of chemical and photochemical reactions on metal oxides: bridging the materials gap. *Chem. Soc. Rev.* **46,** 1875–1932 (2017).

68. Fernández-García, M., Martínez-Arias, A., Hanson, J. C. & Rodriguez, J. A. Nanostructured oxides in chemistry: Characterization and properties. *Chem. Rev.* **104,** 4063–4104 (2004).

69. Mahapatra, M. *et al.* The Behavior of Inverse Oxide/Metal Catalysts: CO Oxidation and Water-gas Shift Reactions over ZnO/Cu(111) Surfaces. *Surf. Sci.* **681,** 116–121 (2018).

70. Chen, Y. Z. *et al.* Singlet oxygen-engaged selective photo-oxidation over pt nanocrystals/porphyrinic MOF: The roles of photothermal effect and pt electronic state. *J. Am. Chem. Soc.* **139,** 2035–2044 (2017).

71. Martínez-Suárez, L., Frenzel, J. & Marx, D. Cu/ZnO nanocatalysts in response to environmental conditions: Surface morphology, electronic structure, redox state and CO2 activation. *Phys. Chem. Chem. Phys.* **16,** 26119–26136 (2014).

72. Kattel, S., Ramírez, P. J., Chen, J. G., Rodriguez, J. A. & Liu, P. Active sites for CO_2 hydrogenation to methanol on Cu/ZnO catalysts. *Science (80-.).* **355,** 1296–1299 (2017).

73. Chen, H. *et al.* CO and H_2 Activation over g-ZnO Layers and w-ZnO(0001). *ACS Catal.* 1373–1382 (2019). doi:10.1021/acscatal.8b03687

74. Wang, Y. & Wöll, C. IR spectroscopic investigations of chemical and photochemical reactions on metal oxides: Bridging the materials gap. *Chem. Soc. Rev.* **46,** 1875–1932 (2017).

75. Li, N. *et al.* Size Effects of ZnO Nanoparticles in Bifunctional Catalysts for Selective Syngas Conversion. *ACS Catal.* 960–966 (2019). doi:10.1021/acscatal.8b04105

76. Thang, H. V., Tosoni, S. & Pacchioni, G. Evidence of Charge Transfer to Atomic and Molecular Adsorbates on ZnO/X(111) (X = Cu, Ag, Au) Ultrathin Films. Relevance for Cu/ZnO Catalysts. *ACS Catal.* **8,** 4110–4119 (2018).

77. Limo, M. J. *et al.* Interactions between Metal Oxides and Biomolecules: From Fundamental Understanding to Applications. *Chem. Rev.* **118,** 11118–11193 (2018).

78. Zhang, H. *et al.* Influence of ZnO facets on Pd/ZnO catalysts for methanol steam reforming. *ACS Catal.* **4,** 2379–2386 (2014).

79. Bu, Y., Weststrate, C. J., Niemantsverdriet, J. W. & Fredriksson, H. O. A. Role of ZnO and CeOx in Cu-Based model catalysts in activation of h2O and CO2 dynamics studied by in situ ultraviolet−Visible and x-ray photoelectron spectroscopy. *ACS Catal.* **6,** (2016).

80. Ayastuy, J. L., Gutiérrez-Ortiz, M. A., González-Marcos, J. A., Aranzabal, A. & González-Velasco, J. R. Kinetics of the Low-Temperature WGS Reaction over a CuO/ZnO/Al 2 O 3 Catalyst. *Ind. Eng. Chem. Res.* **44,** 41–50 (2005).

81. Jiao, F. *et al.* Selective conversion of syngas to light olefins-supporting material. *Science (80-.).* **351,** 1065–1068 (2016).

82. Cheng, K. *et al.* Direct and Highly Selective Conversion of Synthesis Gas into

Lower Olefins: Design of a Bifunctional Catalyst Combining Methanol Synthesis and Carbon-Carbon Coupling. *Angew. Chemie - Int. Ed.* **55,** 4725–4728 (2016).

83. Mahapatra, M. *et al.* Growth, Structure and Catalytic Properties of ZnO_x Grown on CuO_x /Cu(111) Surfaces. *J. Phys. Chem. C* acs.jpcc.8b09243 (2018). doi:10.1021/acs.jpcc.8b09243

84. Senanayake, S. D. *et al.* Hydrogenation of CO2 to Methanol on CeOx/Cu(111) and ZnO/Cu(111) Catalysts: Role of the Metal-Oxide Interface and Importance of Ce3+ Sites. *J. Phys. Chem. C* **120,** 1778–1784 (2016).

85. Martin, O. *et al.* Operando Synchrotron X-ray Powder Diffraction and Modulated-Excitation Infrared Spectroscopy Elucidate the CO2Promotion on a Commercial Methanol Synthesis Catalyst. *Angew. Chemie - Int. Ed.* **55,** 11031–11036 (2016).

86. Martínez-Suarez, L., Siemer, N., Frenzel, J. & Marx, D. Reaction Network of Methanol Synthesis over Cu/ZnO Nanocatalysts. *ACS Catal.* **5,** 4201–4218 (2015).

87. Roy, S., Cherevotan, A. & Peter, S. C. Thermochemical CO2Hydrogenation to Single Carbon Products: Scientific and Technological Challenges. *ACS Energy Lett.* **3,** 1938–1966 (2018).

88. Li, W. *et al.* Low Temperature CO_2 Methanation: ZIF-67-Derived Co-Based Porous Carbon Catalysts with Controlled Crystal Morphology and Size. *ACS Sustain. Chem. Eng.* **5,** 7824–7831 (2017).

89. Muroyama, H. *et al.* Carbon dioxide methanation over Ni catalysts supported on various metal oxides. *J. Catal.* **343,** 178–184 (2016).

90. Díez-Ramírez, J. *et al.* Effect of support nature on the cobalt-catalyzed

CO2hydrogenation. *J. CO2 Util.* **21,** 562–571 (2017).

91. Vidal, A. B. *et al.* CO 2 activation and methanol synthesis on novel Au/TiC and Cu/TiC catalysts. *J. Phys. Chem. Lett.* **3,** 2275–2280 (2012).

92. Spanjers, C. S., Sim, R. S., Sturgis, N. P., Kabius, B. & Rioux, R. M. In situ spectroscopic characterization of Ni<inf>1- x</inf>Zn<inf>x</inf>/ZnO catalysts and their selectivity for acetylene semihydrogenation in excess ethylene. *ACS Catal.* **5,** 3304–3315 (2015).

93. Divins, N. J., Angurell, I., Escudero, C., Perez-Dieste, V. & Llorca, J. Influence of the support on surface rearrangements of bimetallic nanoparticles in real catalysts. *Science (80-.).* **346,** 620–623 (2014).

94. Wang, X., Shi, H. & Szanyi, J. Controlling selectivities in CO2 reduction through mechanistic understanding. *Nat. Commun.* **8,** 513 (2017).

95. Stacchiola, D. J. Tuning the Properties of Copper-Based Catalysts Based on Molecular in Situ Studies of Model Systems. *Acc. Chem. Res.* **48,** 2151–2158 (2015).

96. Wehrens-dijksma, M. & Notten, P. H. L. Electrochemical Quartz Microbalance characterization of Ni (OH) 2 -based thin film electrodes. **51,** 3609–3621 (2006).

97. Wang, X. *et al.* Environmental Science Nano. 190–202 (2016). doi:10.1039/c5en00191a

98. Liu, H., Li, P., Lu, B., Wei, Y. & Sun, Y. Journal of Solid State Chemistry Transformation of ferrihydrite in the presence or absence of trace Fe (II): The effect of preparation procedures of ferrihydrite. *J. Solid State Chem.* **182,** 1767–1771 (2009).

99. Youn, D. H. *et al.* One-pot synthesis of NiFe layered double hydroxide/reduced

graphene oxide composite as an efficient electrocatalyst for electrochemical and photoelectrochemical water oxidation. *J. Power Sources* **294,** 437–443 (2015).

100. Jia, Y. *et al.* A Heterostructure Coupling of Exfoliated Ni–Fe Hydroxide Nanosheet and Defective Graphene as a Bifunctional Electrocatalyst for Overall Water Splitting. *Adv. Mater.* **29,** 1–8 (2017).

101. Long, X. *et al.* A strongly coupled graphene and FeNi double hydroxide hybrid as an excellent electrocatalyst for the oxygen evolution reaction. *Angew. Chemie - Int. Ed.* **53,** 7584–7588 (2014).

102. Song, F. & Hu, X. Exfoliation of layered double hydroxides for enhanced oxygen evolution catalysis. *Nat. Commun.* **5,** 1–9 (2014).

103. Gong, M. *et al.* An advanced Ni-Fe layered double hydroxide electrocatalyst for water oxidation. *J. Am. Chem. Soc.* **135,** 8452–8455 (2013).

104. Han, N., Zhao, F. & Li, Y. Ultrathin nickel–iron layered double hydroxide nanosheets intercalated with molybdate anions for electrocatalytic water oxidation. *J. Mater. Chem. A* **3,** 16348–16353 (2015).

105. Chen, J. Y. C. *et al.* Operando Analysis of NiFe and Fe Oxyhydroxide Electrocatalysts for Water Oxidation: Detection of Fe4+by Mössbauer Spectroscopy. *J. Am. Chem. Soc.* **137,** 15090–15093 (2015).

106. Huang, J. *et al.* Improving Electrocatalysts for Oxygen. *ACS Energy Lett.* **3,** 1698–1707 (2018).

107. Stevens, M. B., Trang, C. D. M., Enman, L. J., Deng, J. & Boettcher, S. W. Reactive Fe-Sites in Ni/Fe (Oxy)hydroxide Are Responsible for Exceptional Oxygen Electrocatalysis Activity. *J. Am. Chem. Soc.* **139,** 11361–11364 (2017).

108. Friebel, D. *et al.* Identification of highly active Fe sites in (Ni,Fe)OOH for

electrocatalytic water splitting. *J. Am. Chem. Soc.* **137,** 1305–1313 (2015).

109. Rana, A. K. *et al.* Search for Origin of Room Temperature Ferromagnetism Properties in Ni-Doped ZnO Nanostructure. *ACS Appl. Mater. Interfaces* **9,** 7691–7700 (2017).

110. Zhang, Y.-Z. *et al.* Porous hollow Co $_3$ O $_4$ with rhombic dodecahedral structures for high-performance supercapacitors. *Nanoscale* **6,** 14354–14359 (2014).

111. Gao, M. *et al.* Porous ZnO-Coated Co3O4Nanorod as a High-Energy-Density Supercapacitor Material. *ACS Appl. Mater. Interfaces* **10,** 23163–23173 (2018).

112. Zhang, F. *et al.* In Situ Elucidation of the Active State of Co-CeOxCatalysts in the Dry Reforming of Methane: The Important Role of the Reducible Oxide Support and Interactions with Cobalt. *ACS Catal.* **8,** 3550–3560 (2018).

113. Da Costa-Serra, J. F., Guil-López, R. & Chica, A. Co/ZnO and Ni/ZnO catalysts for hydrogen production by bioethanol steam reforming. Influence of ZnO support morphology on the catalytic properties of Co and Ni active phases. *Int. J. Hydrogen Energy* **35,** 6709–6716 (2010).

114. Den Breejen, J. P. *et al.* On the origin of the cobalt particle size effects in Fischer-Tropsch catalysis. *J. Am. Chem. Soc.* **131,** 7197–7203 (2009).

115. Bezemer, G. L. *et al.* Cobalt particle size effects in the Fischer-Tropsch reaction studied with carbon nanofiber supported catalysts. *J. Am. Chem. Soc.* **128,** 3956–3964 (2006).

116. Vogt, C. *et al.* Unravelling structure sensitivity in CO2hydrogenation over nickel. *Nat. Catal.* **1,** 127–134 (2018).

117. Zhou, G. *et al.* Role of surface Ni and Ce species of Ni/CeO2catalyst in CO2methanation. *Appl. Surf. Sci.* **383,** 248–252 (2016).

118. Heine, C., Lechner, B. A. J., Bluhm, H. & Salmeron, M. Recycling of CO2: Probing the Chemical State of the Ni(111) Surface during the Methanation Reaction with Ambient-Pressure X-Ray Photoelectron Spectroscopy. *J. Am. Chem. Soc.* **138,** 13246–13252 (2016).

119. Porosoff, M. D., Yan, B. & Chen, J. G. Catalytic reduction of CO2by H2for synthesis of CO, methanol and hydrocarbons: Challenges and opportunities. *Energy Environ. Sci.* **9,** 62–73 (2016).

120. Rodriguez, J. A., Hanson, J. C., Stacchiola, D. & Senanayake, S. D. In situ/operando studies for the production of hydrogen through the water-gas shift on metal oxide catalysts. *Phys. Chem. Chem. Phys.* **15,** 12004 (2013).

121. Bentrup, U. Combining in situ characterization methods in one set-up: looking with more eyes into the intricate chemistry of the synthesis and working of heterogeneous catalysts. *Chem. Soc. Rev.* **39,** 4718 (2010).

122. Frenkel, A. I., Rodriguez, J. A. & Chen, J. G. Synchrotron techniques for in situ catalytic studies: Capabilities, challenges, and opportunities. *ACS Catal.* **2,** 2269–2280 (2012).

123. Zhang, S. *et al.* In-situ studies of nanocatalysis. *Acc. Chem. Res.* **46,** 1731–1739 (2013).

124. Frenkel, A. I. *et al.* Combining X-ray absorption and X-ray diffraction techniques for in situ studies of chemical transformations in heterogeneous catalysis: Advantages and limitations. *J. Phys. Chem. C* **115,** 17884–17890 (2011).

125. Takagi, Y. *et al.* X-ray photoelectron spectroscopy under real ambient pressure conditions. *Appl. Phys. Express* **10,** (2017).

126. Palomino, R. M. *et al.* Interfaces in heterogeneous catalytic reactions: Ambient

pressure XPS as a tool to unravel surface chemistry. *J. Electron Spectros. Relat. Phenomena* (2016). doi:10.1016/j.elspec.2017.04.006

127. Starr, D. E., Liu, Z., Hävecker, M., Knop-Gericke, A. & Bluhm, H. Investigation of solid/vapor interfaces using ambient pressure X-ray photoelectron spectroscopy. *Chem. Soc. Rev.* **42,** 5833 (2013).

128. Liu, X., Yang, W. & Liu, Z. Recent progress on synchrotron-based in-situ soft X-ray spectroscopy for energy materials. *Adv. Mater.* **26,** 7710–7729 (2014).

129. Alayoglu, S. *et al.* In situ surface and reaction probe studies with model nanoparticle catalysts. *ACS Catal.* **2,** 2250–2258 (2012).

130. Stoerzinger, K. A., Hong, W. T., Crumlin, E. J., Bluhm, H. & Shao-Horn, Y. Insights into Electrochemical Reactions from Ambient Pressure Photoelectron Spectroscopy. *Acc. Chem. Res.* **48,** 2976–2983 (2015).

131. Briggs, D. X: X-Ray Photoelectron Spectroscopy. *Handb. Adhes. Second Ed.* 621–622 (2005). doi:10.1002/0470014229.ch22

132. Melaet, G. *et al.* Evidence of highly active cobalt oxide catalyst for the Fischer-Tropsch synthesis and CO2 hydrogenation. *J. Am. Chem. Soc.* **136,** 2260–2263 (2014).

133. Ni, Y. *et al.* Selective conversion of CO2and H2into aromatics. *Nat. Commun.* **9,** 1–7 (2018).

134. Jacques, S. D. M. *et al.* Recent progress in the use of in situ X-ray methods for the study of heterogeneous catalysts in packed-bed capillary reactors. *Catal. Today* **145,** 204–212 (2009).

135. Rodriguez, J. A. *et al.* In-situ characterization of water-gas shift catalysts using time-resolved X-ray diffraction. *Catal. Today* **145,** 188–194 (2009).

136. Sheela, G., Pushpavanam, M. & Pushpavanam, S. Zinc-nickel alloy electrodeposits for water electrolysis. *Int. J. Hydrogen Energy* **27,** 627–633 (2002).

137. Yang, J. M., Gou, S. P. & Sun, I. W. Single-step large-scale and template-free electrochemical growth of Ni-Zn alloy filament arrays from a zinc chloride based ionic liquid. *Chem. Commun.* **46,** 2686–2688 (2010).

RESUMÉ

Thaylan Pinheiro Araújo

Born 17 July 1994 in Maranhão, Brazil.

EDUCATION

University of São Paulo, USP, (Department of Fundamental Chemistry), São Paulo, Brazil

M.S. Candidate in Chemistry 2017-current
São Paulo Research Foundation (FAPESP) Master Fellowship
Advisor: *Prof. Pedro H. C. Camargo, Ph.D.*

Brookhaven National Laboratory, BNL, Chemistry Division, Upton, New York, The USA

FAPESP MSc. Exchange Student 05/2018–10/2018
Advisor: Prof. *José A. Rodriguez, Ph.D, Senior Chemist*

Federal University of Maranhão, UFMA, Department of Chemistry, São Luís, Brazil

B.S. in Chemistry 08/2011–01/2017
Advisor: Prof. Auro Atsushi Tanaka, Ph.D.

National University of Ireland, School of Chemistry, Galway, Ireland

Science without Borders Exchange Student 09/2013–12/2014
Advisor: Profa. Andrea Erxleben, Ph.D.

Federal Institute of Education, Science and Technology of Maranhão, IFMA, Brazil

Habilitation (professional qualification) in Biofuels and Chemistry Laboratory Technician 03/ 2008-12/2010

OCCUPATION

M. Sc. Student

Universidade de São Paulo, São Paulo, Brazil.

CNPq Fellowship, 03/2017 - 06/2017

FAPESP Fellowship, 07/2017 – 02/2019.

RESEARCH EXPERIENCE

2017- Currretly: University of São Paulo, São Paulo, São Paulo, Brazil

FAPESP M.Sc. Research Fellow, Department of Fundamental Chemistry

(Advisor: Prof. Pedro H. C. Camargo, Ph.D.)

M.Sc. research project: *'Hybrid nanomaterials for energy conversion: integrating plasmonic nanostructures and photoluminescent nanomaterials'*

2018-2018: Brookhaven National Laboratory, BNL, Upton, New York, The USA

FAPESP M.Sc. Exchange Student, Chemistry Division

(Advisor: Prof. José A. Rodruiguez, Ph.D.)

Research Proposal: '*In situ/operando* investigations of the CO_2 hydrogenation process on Ni and Co/ZnO surfaces: Probing catalytically important properties.'

2015-2016: Federal University of Maranhão, São Luís, Maranhão, Brazil

CNPq Undergraduate Research Fellow, Department of Chemistry

(Advisor: Prof. Auro Atsushi Tanaka, Ph.D)

- Fabrication of modified electrode composites using graphene oxide and carbon nanotubes combined with phthalocyanine, porphyrin, and/or molecularly imprinted polymers.
- Application of such modified electrode composites on the electrochemical detection of important environmental and pharmaceutical compounds.

2014: National University of Ireland, Galway, Ireland

CAPES Undergraduate Research Fellow, School of Chemistry

(Advisor: Prof. Andrea Erxleben, Ph.D)

Final Project: *'DNA binding, cleavage and cytotoxicity of a novel dimetallic Fe(III) triaza-cyclononane complex.'*

2012-2013: Federal University of Maranhão, São Luís, Maranhão, Brazil

FAPEMA Undergraduate Research Fellow, Department of Chemistry

(Advisor: Prof. Auro Atsushi Tanaka, Ph.D)

- Synthesis of hybrid nanomaterials based on manganese phthalocyanine as well as its oxide derivatives with doped and undoped nitrogen-carbonaceous supports;

- Investigation of such hybrid nanomaterials as electrocatalysts for the oxygen reduction reaction (ORR) in direct-methanol fuel cells (DMFCs);

PUBLICATIONS

1. *'DNA binding, cleavage and cytotoxicity of a novel dimetallic Fe(III) triaza-cyclononane complex.'* **T. P. Araujo**, V. Gandinc, P. Kavanagh, J. P. Braude, L. Nodari, D. Montagner and A. Erxleben. **Inorganica Chimica Acta**. Volume 452, 1 October **2016**, Pages 170-175. (doi: 10.1016/j.ica.2016.02.044)

2. *'Fast quantification of α-lipoic acid in biological samples and dietary supplements using batch injection analysis with amperometric detection*.' L. N. S. Pereira, I. S. Silva, **T. P. Araújo**, A. A. Tanaka, L. Angnes. ***Talanta***. Volume 154, 1 July **2016**, Pages 249-254. (doi: 10.1016/j.talanta.2016.03.046)

3. *'Controlling Reaction Selectivity over Hybrid Plasmonic Nanocatalysts.'*J. Quiroz, E. C. M. Barbosa, **T. P. Araujo**, J. L. Fiorio, Y. Wang, Y. Zou, T. Mou, T. V. Alves, D.C. de Oliveira, B. Wang, S. J. Haigh, L. M. Rossi, and P. H. C. Camargo. **Nano Lett**., 2018, 18 (11), pp 7289–7297. (doi:10.1021/acs.nanolett.8b03499)

4. *'Understanding Plasmonic Catalysis with Controlled Nanomaterials based on Catalytic and Plasmonic Metals.*' **T. P. Araujo***, J. Quiroz*, E.C.M. Barbosa, and P.H.C. Camargo. Current Opinion in Colloid & Interface Science. (*Invited review paper) accepted*. January, **2019.**

POSTER AND ORAL PRESENTATIONS

1. Y. A. VIEIRA, **T. P. ARAÚJO**, I. S. DA SILVA, A. A. TANAKA. Development of electrochemical sensor based on graphene oxide modified with cobalt porphyrin for the detection of 2,6-dichloro- 1,4-benzoquinone. In: XIX Simpósio Brasileiro de Eletroquímica e Eletroanalítica, 2013, Natal (RN). Anais do XXI SIBEE, 2017. v. 1. p. 1-3. , Natal-RN.

2. ARAUJO, J. A. ; **ARAÚJO, T. P**. ; LOPES, I. C. ; TANAKA, S. M. C. N. ; SILVA, I. S. . Triclosan detection on a molercularly imprinted carbon nanotube sensor. In: 16th Topical Meeting of the International Society of Electrochemistry, 2015, Angra dos Reis. Electrochemical Properties and Applications of Advanced Carbon Materials, 2015.

3. RODRIGUES, A. P. ; LOPES, I. C. ; **ARAÚJO, T. P.** ; TANAKA, S. M. C. N. ; TANAKA, AURO ATSUSHI . Carboxylated -cyclodextrin-reduced graphene oxide for the voltametric determination of diuron herbicide. In: 16th Topical Meeting of the International Society of Electrochemistry, 2015, Angra dos Reis. Electrochemical Properties and Applications of Advanced Carbon Materials, 2015.

4. **ARAÚJO, T. P.** ; CASTRO, U. J. ; TANAKA, AURO ATSUSHI . Estudos da redução de oxigênio sobre eletrodos MnPc/C na presença de metanol em soluções aquosas alcalinas,. In: XIX Simpósio Brasileiro de Eletroquímica e Eletroanalítica, 2013, Campos do Jordão (SP). Anais do XIX SIBEE, 2013. v. 1. p. 1-3.

5. **ARAÚJO, T. P**. ; Araujo, Jeovan A. de ; BRITO, N. M. ; ARAÚJO, A. B. . Potabilização de água contendo Bisfenol-A após aplicação de Método de Tratamento Avançado. In: 35° Reunião Anual da Sociedade Brasileira de Química, 2012, Águas de Lindóia - SP. 35°RASBQ, 2012.

6. MORAIS, G. M. ; **ARAÚJO, T. P**. ; MELO, S. M. ; BRITO, N. M. ; ARAÚJO, A. B. .FOTODEGRADAÇÃO DE BISFENOL-A UTILIZANDO CATALISADORES DE Ag/TiO2. In: 16º ENQA | Encontro Nacional de Química Analítica, 2011, Campos do Jordão-SP. 16º ENQA | Encontro Nacional de Química Analítica, 2011.